RNA (2001), *7*:1317–1334. Cambridge University Press. Printed in the USA.

DOI: 10.1017.S1355838201010640

Dbp9p, a putative ATP-dependent RNA helicase involved in 60S-ribosomal-subunit biogenesis, functionally interacts with Dbp6p

MARIE-CLAIRE DAUGERON,[1,2]* DIETER KRESSLER,[1,3]* and PATRICK LINDER[1]

[1]Département de Biochimie médicale, Centre Médical Universitaire, Université de Genève, CH-1211 Genève 4, Switzerland

ABSTRACT

Ribosome synthesis is a highly complex process and constitutes a major cellular activity. The biogenesis of this ribonucleoprotein assembly requires a multitude of protein *trans*-acting factors including several putative ATP-dependent RNA helicases of the DEAD-box and related protein families. Here we show that the previously uncharacterized *Saccharomyces cerevisiae* open reading frame YLR276C, hereafter named *DBP9* (DEAD-box protein 9), encodes an essential nucleolar protein involved in 60S-ribosomal-subunit biogenesis. Genetic depletion of Dbp9p results in a deficit in 60S ribosomal subunits and the appearance of half-mer polysomes. This terminal phenotype is likely due to the instability of early pre-ribosomal particles, as evidenced by the low steady-state levels and the decreased synthesis of the 27S precursors to mature 25S and 5.8S rRNAs. In agreement with a role of Dbp9p in 60S subunit synthesis, we find that increased Dbp9p dosage efficiently suppresses certain *dbp6* alleles and that *dbp6*/*dbp9* double mutants show synthetic lethality. Furthermore, Dbp6p and Dbp9p weakly interact in a yeast two-hybrid assay. Altogether, our findings indicate an intimate functional interaction between Dbp6p and Dbp9p during the process of 60S-ribosomal-subunit assembly.

Keywords: DEAD-box proteins; multicopy suppressor; nucleolus; ribosome biosynthesis; yeast

INTRODUCTION

Ribosomes are one of the largest and undoubtedly most complex macromolecular assemblies (≥3 MDa in eukaryotes). From the recently solved structure of a prokaryotic large ribosomal subunit, it could be established that the ribosome is a ribozyme; ribosomal proteins (r-proteins) are absent from the active site peptidyl transferase center and they rather seem to be important for conferring structural stability (Ban et al., 2000; Nissen et al., 2000). The synthesis of ribosomes represents a major cellular activity. It has been calculated that a rapidly growing *Saccharomyces cerevisiae* cell contains approximately 200,000 ribosomes and, with a generation time of about 90 min, must produce more than 2,000 ribosomes per minute (Warner, 1999). Therefore, it is not surprising that eukaryotic cells have evolved intricate mechanisms, including the requirement of a large number of *trans*-acting factors (see below), to ensure the accurate synthesis of this massive amount of translation competent ribosomes. Insights into the process of ribosome biogenesis have been so far mainly gathered through the combination of molecular genetic and biochemical approaches in the yeast *S. cerevisiae* (Kressler et al., 1999b; Venema & Tollervey, 1999). The high conservation of the basic outline of eukaryotic ribosome synthesis makes *S. cerevisiae* the ideal model organism to further our understanding of this process (Eichler & Craig, 1994).

In *S. cerevisiae*, the large 60S ribosomal subunits are composed of 46 r-proteins and three rRNA species (25S, 5.8S, and 5S), and the small 40S ribosomal subunits contain 32 r-proteins and the 18S rRNA (Planta & Mager, 1998; Woolford & Warner, 1991). The early steps of ribosome synthesis take place in a specialized subnuclear compartment termed the nucleolus (Mélèse & Xue, 1995; Olson et al., 2000; Scheer & Hock, 1999). There, the ribosomal DNA is transcribed by RNA poly-

Reprint requests to: Patrick Linder, Département de Biochimie médicale, Centre Médical Universitaire, Université de Genève, 1, rue Michel-Servet, CH-1211 Genève 4, Switzerland; e-mail: Patrick.Linder@medecine.unige.ch.

[2]Present address: Equipe "Epissage et dégradation des ARNs messagers eucaryotes", Bat 24 CGM CNRS, Avenue de la Terrasse, 91198 Gif sur Yvette, Cedex, France.

[3]Present address: Division of Biochemistry, Biozentrum of the University of Basel, Klingelbergstrasse 70, CH-4056 Basel, Switzerland.

*The first two authors contributed equally to this work; the order has been defined by tossing a coin.

merase I and RNA polymerase III into a 35S and a 5S pre-rRNA, respectively, which undergo covalent modifications and endo- and exonucleolytic cleavage reactions (Fig. 1). The maturation of pre-rRNAs is intimately linked to their assembly with r-proteins. Many r-proteins assemble early onto the 35S pre-rRNA to form a 90S pre-ribosomal particle. From this particle, 66S and 43S pre-ribosomes containing the 27S and 20S pre-rRNAs, respectively, are formed (Trapman et al., 1975). The 43S pre-ribosome is rapidly exported to the cytoplasm, where the final maturation step in the synthesis of the 18S rRNA takes place (Udem & Warner, 1973; Trapman & Planta, 1976). The 66S particle remains in the nucleus until exonucleolytic trimming of the 7S precursor to mature 5.8S rRNA is completed (Trapman et al., 1976) and some final nucleoplasmic assembly events

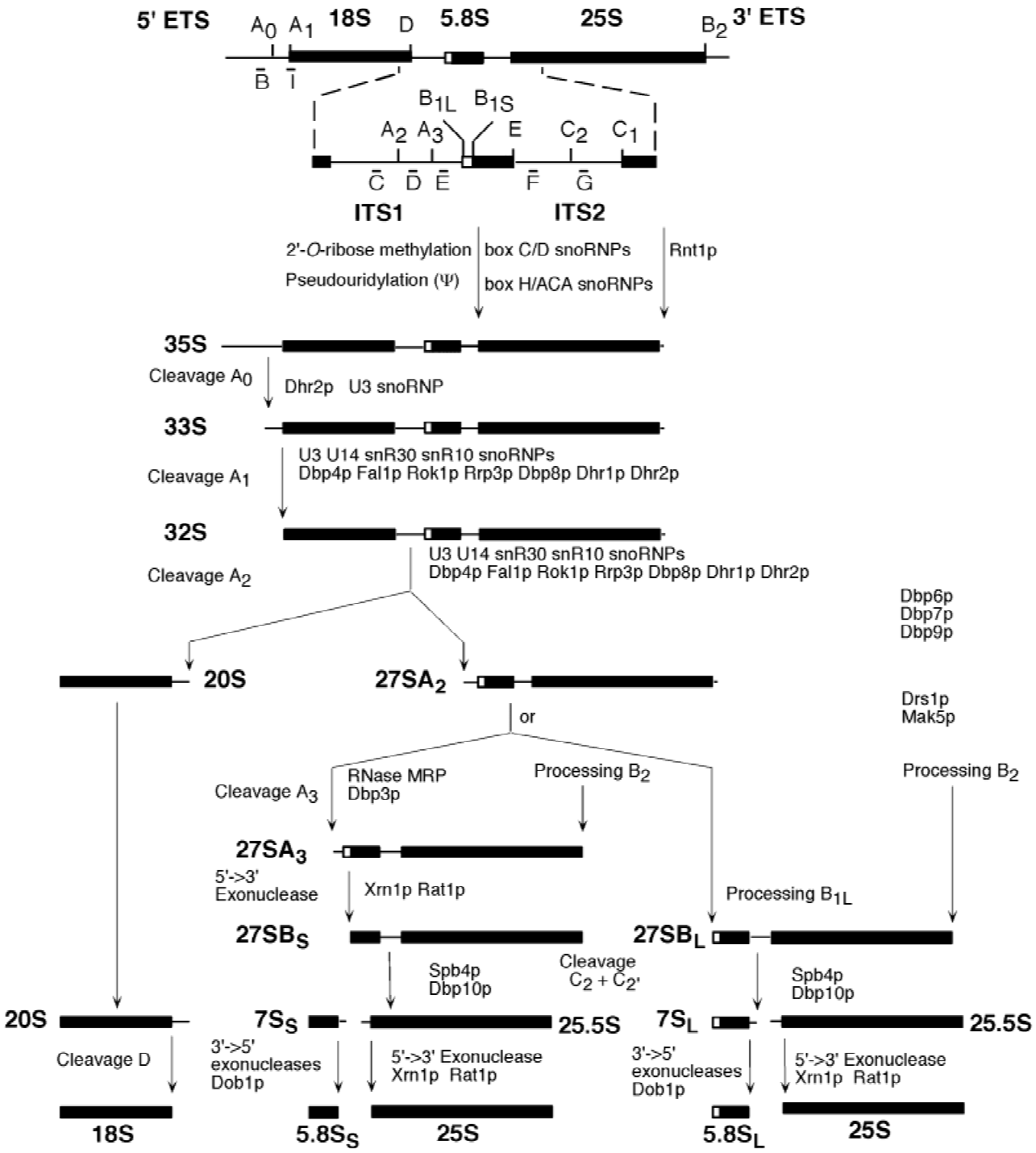

FIGURE 1. (*Legend on facing page.*)

have generated export-competent large ribosomal subunits (Kressler et al., 1999a; Aitchison & Rout, 2000; Ho et al., 2000).

Maturation of the pre-rRNAs and their concomitant assembly with r-proteins requires, besides small nucleolar RNAs (snoRNAs), a multitude of different protein *trans*-acting factors (≥65), such as components of small ribonucleoprotein particles (snoRNPs), rRNA modifying enzymes, endo- and exonucleases, and putative RNA helicases (Kressler et al., 1999b; Venema & Tollervey, 1999). The putative RNA helicases of the DEAD-box and related protein families represent the largest class of protein *trans*-acting factors involved in ribosome biogenesis. These ubiquitous protein families are defined by several evolutionarily conserved motifs, and their members are involved in various RNA metabolic processes, including pre-mRNA splicing, mRNA export, translation initiation, RNA degradation, and ribosome biogenesis (de la Cruz et al., 1999). Many of these proteins possess an RNA-dependent ATPase activity, which is sometimes only stimulated by specific RNA substrates (Fuller-Pace et al., 1993; O'Day et al., 1996). So far ATP-dependent RNA helicase activity could only be shown for a few of them (discussed in Iost et al., 1999), and furthermore, a processive RNA unwinding activity has solely been reported for the vaccinia virus NPH-II helicase (Jankowsky et al., 1999). Therefore, one collectively refers to these proteins as putative ATP-dependent RNA helicases (de la Cruz et al., 1999). Considering the RNA structures—mostly short inter- and intramolecular RNA duplexes—that are encountered by putative RNA helicases during, for example, spliceosome rearrangements or ribosome biogenesis (Staley & Guthrie, 1998; Venema & Tollervey, 1999), it is clear that a true "helicase" activity is not even needed. Moreover, and as suggested by recent reports (Chen et al., 2001; Jankowsky et al., 2001; Kistler & Guthrie, 2001; Linder et al., 2001), it is very likely that the putative RNA helicases involved in ribosome biogenesis are not only required for the ATP-dependent dissociation of RNA–RNA substrates, but that they also actively modulate specific RNA–protein or even protein–protein interactions (Lorsch & Herschlag, 1998a, 1998b). These structural rearrangements ensure efficient and accurate ribosome synthesis. In the absence of such a putative RNA helicase, the lack or retardation of the required structural changes may lead to an abortive assembly, which can entail either disassembly of pre-ribosomal particles and destabilization of pre-rRNA intermediates (Kressler et al., 1998, and see below) or accumulation of pre-ribosomal particles and stabilization of pre-rRNA intermediates (de la Cruz et al., 1998; Burger et al., 2000).

To better understand the cellular roles of DEAD-box proteins in general and their function in ribosome biogenesis in particular, we set out to characterize the *S. cerevisiae* open reading frame (ORF) YLR276C, which is hereafter called *DBP9* (DEAD-box protein 9). We show that Dbp9p is an essential nucleolar protein that is required for ribosome biogenesis. In vivo depletion of Dbp9p entails reduced synthesis of the 27SB precursor to mature 25S and 5.8S rRNA, which leads ter-

FIGURE 1. Pre-rRNA processing in *S. cerevisiae*. The RNA polymerase I transcribed pre-rRNA contains the sequences for the mature 18S, 5.8S, and 25S rRNAs that are separated by two internal transcribed spacer sequences, ITS1 and ITS2, and flanked by two external transcribed spacer sequences, 5′ ETS and 3′ ETS. The mature rRNA species are shown as bars and the transcribed spacer sequences as lines. The processing sites and their locations as well as the various probes used are indicated. The primary RNA pol I transcript undergoes covalent modifications (2′-*O*-ribose methylation and pseudouridylation), and it is processed at its 3′ end to yield the 35S pre-rRNA, which is the longest detectable precursor. Early associating 40S and 60S r-proteins as well as *trans*-acting factors (proteins and snoRNAs) assemble on this precursor to form a 90S pre-ribosomal particle (90S RNP). The 35S pre-rRNA is first cleaved at the U3 snoRNP dependent site A_0 to generate the 33S pre-rRNA. This molecule is subsequently processed at sites A_1 and A_2; the latter cleavage results in the separation of the pre-rRNAs destined for the small and large ribosomal subunits and allows the 90S RNP to separate into a 43S RNP and a 66S RNP. The early pre-rRNA cleavages A_0 to A_2 require snoRNP components and the putative ATP-dependent RNA helicases Dbp4p, Fal1p, Rok1p, Rrp3p, Dbp8p, Dhr1p, and Dhr2p. The 43S RNP is exported to the cytoplasm, where endonucleolytic cleavage of the 20S precursor at site D yields the mature 18S rRNA. Other nucleolar assembly reactions probably occur concomitantly to the early cleavages and include incorporation of the Rpl5p-5S RNP and of later associating r-proteins. The structural rearrangements within early or intermediate pre-ribosomal particles are likely to require the putative ATP-dependent RNA helicases Dbp6p, Dbp7p, and as shown here Dbp9p. The $27SA_2$ precursor within the 66S RNP is processed by two alternative pathways that both lead to the formation of nuclear pre-60S particles containing the mature 5.8S and 25S rRNAs. In the major pathway, the $27SA_2$ precursor is cleaved at site A_3 by the RNase MRP complex. The putative ATP-dependent RNA helicase Dpb3p assist in this processing step. The $27SA_3$ precursor is exonucleolytically digested $5' \rightarrow 3'$ up to site B_{1S} to yield the $27SB_S$ precursor, a reaction requiring the exonucleases Xrn1p and Rat1p. A minor pathway processes the $27SA_2$ molecule at site B_{1L}, producing the $27SB_L$ pre-rRNA. While processing at site B_1 is completed, the 3′ end of mature 25S rRNA is generated by processing at site B_2. The subsequent ITS2 processing of both 27SB species appears to be identical. Cleavages at sites C_2 and $C_{2'}$ release the 7S pre-rRNA and a 25.5S precursor, which is $5' \rightarrow 3'$ exonucleolytically digested by Xrn1p and Rat1p to yield the mature 25S rRNA. Mutations in the *SPB4* and *DBP10* genes affect cleavage at site C_2 and $C_{2'}$. The 7S pre-rRNA undergoes exosome-dependent $3' \rightarrow 5'$ exonuclease digestion to the 3′ end of the mature 5.8S rRNA. It has been proposed that Dob1p/Mtr4p, a putative ATP-dependent RNA helicase, assists the exosome activity. The exact roles of the putative RNA helicases Drs1p and Mak5p have not been defined. For reviews on pre-rRNA processing and *trans*-acting factors involved in this process see Kressler et al. (1999b) and Venema and Tollervey (1999).

minally to a net deficit in 60S ribosomal subunits. Interestingly, increased dosage of Dbp9p suppresses certain *dbp6* alleles and *dbp6/dbp9* double mutants show synthetic enhancement phenotypes. Moreover, Dbp6p and Dbp9p weakly interact in a yeast two-hybrid assay. Together, our findings indicate an intimate functional interaction between Dbp6p and Dbp9p during early steps of 60S-ribosomal-subunit assembly.

RESULTS

Dbp9p is a putative RNA helicase essential for vegetative growth

DBP9 (*YLR276C*) is located on the left arm of chromosome XII and encodes a basic protein of 594 amino acids with a predicted mass of 68 kDa and a predicted pI of 9.36. The main sequence feature of Dbp9p is the presence of the eight conserved motifs that constitute the so-called RNA helicase core region characteristic of DEAD-box proteins (de la Cruz et al., 1999). Blast searches with Dbp9p reveal highly similar proteins from various species including *Schizosaccharomyces pombe* (O93990), *Homo sapiens* (Q9NY93), *Drosophila melanogaster* (O61350), *Arabidopsis thaliana* (Q9SW44), and *Caenorhabditis elegans* (O17157). Based on their homology outside of the helicase core domain, in particular the C-terminal extension, they likely represent real orthologs of Dbp9p (see also Zirwes et al., 2000).

To study the cellular function of Dbp9p, we first disrupted the *DBP9* gene by replacing one entire *DBP9* ORF copy with the HIS3MX6 marker in the diploid W303 strain yielding the heterozygous diploid strain MCD9H. Upon sporulation of this strain, a 2:2 segregation for viability was observed and no His^+ spores were recovered, indicating that *DBP9* is an essential gene. The absolute requirement of *DBP9* for vegetative growth was further confirmed by the analysis of the meiotic progeny of MCD9H transformed with YCplac33-*DBP9*. Mostly tetrads of four viable spores were recovered, and all the His^+ spores showed a complete lack of growth on 5-fluoroorotic acid (5-FOA)-containing plates. Furthermore, under all tested conditions, the haploid strains MCD9H-2D and MCD9H-4C (*dbp9*::HIS3MX6) harboring the plasmid YCplac33-*DBP9* exhibited the same growth behavior as an otherwise isogenic wild-type strain (MCD9H-2A), indicating that the *DBP9* plasmid-borne allele fully complemented the *dbp9*-null allele (Fig. 2A, and data not shown).

A conditional system to study the cellular function of Dbp9p

To study the essential cellular function of Dbp9p, we established a conditional system based on the depletion of Dbp9p by transcriptional repression of a plasmid-borne *GAL::DBP9* fusion gene. In this system, the expression of a N-terminally HA-tagged Dbp9p, driven by the *GAL1-10* promoter, takes place in galactose-based medium but is repressed in glucose-containing medium. The *GAL::DBP9* strain was obtained after transformation of MCD9H-2D [YCplac33-*DBP9*] with the plasmid pAS24-*DBP9* followed by plasmid shuffling on SGal-Leu plates containing 5-FOA. In YPGal medium, the *GAL::DBP9* strain had the same growth behavior as an otherwise isogenic wild-type strain, indicating that the plasmid-borne *GAL::DBP9* allele fully complemented the *dbp9*-null allele. As expected, only residual growth of the *GAL::DBP9* strain was observed on YPD plates (see Fig. 2A). After a shift from YPGal to YPD liquid medium, the growth rate of the *GAL::DBP9* strain remained similar to that of the wild-type strain during at least the first 6 h; it then progressively decreased to reach a doubling time of approximately 8 h after 36 h in YPD medium (Fig. 2B). Monitoring the cellular levels of HA-Dbp9p by western blot analysis indicated that under permissive conditions (YPGal), the protein was overexpressed in the *GAL::DBP9* strain (Fig. 2C, compare lanes 1 and 2) but with ongoing time in YPD, and concomitant with the decrease in growth rate, the cells started to be depleted of HA-Dbp9p (Fig. 2C).

Dbp9p is localized in the nucleolus

As a first hint to the cellular function of Dbp9p, we determined its subcellular localization. For that purpose, we constructed a HA-epitope tagged *DBP9* allele expressed under the control of its cognate promoter. The *HA-DBP9* strain was obtained by transformation of MCD9H-2D [YCplac33-*DBP9*] with YCplac111-*HA-DBP9*, followed by plasmid shuffling on 5-FOA-containing plates. In all the conditions tested, the *HA-DBP9* strain exhibited the same growth behavior as an otherwise isogenic wild-type strain, demonstrating that HA-Dbp9p was fully functional (Fig. 2A and data not shown). Western blot analysis revealed a single protein in a whole-cell lysate of the *HA-DBP9* strain (Fig. 2C), but not from the control strain (data not shown). The detected protein migrated at the expected molecular mass of ~70 kDa. HA-Dbp9p was detected by indirect immunofluorescence following exponential growth in YPD of the HA-Dbp9p harboring strain, using monoclonal mouse anti-HA antibodies and goat anti-mouse fluorescein-conjugated antibodies (Fig. 3C). DNA was stained with DAPI to visualize the nucleus (Fig. 3A). A typical crescent-shaped staining mostly excluded from DAPI-stained areas and characteristic of the nucleolar structure was observed with anti-Nop1p antibodies and goat anti-rabbit rhodamine-conjugated antibodies (Fig. 3B). A highly similar staining was obtained using anti-HA antibodies (Fig. 3C); moreover, merging the anti-Nop1p and the anti-HA micrographs revealed perfect superimposition of both signals, demonstrating that

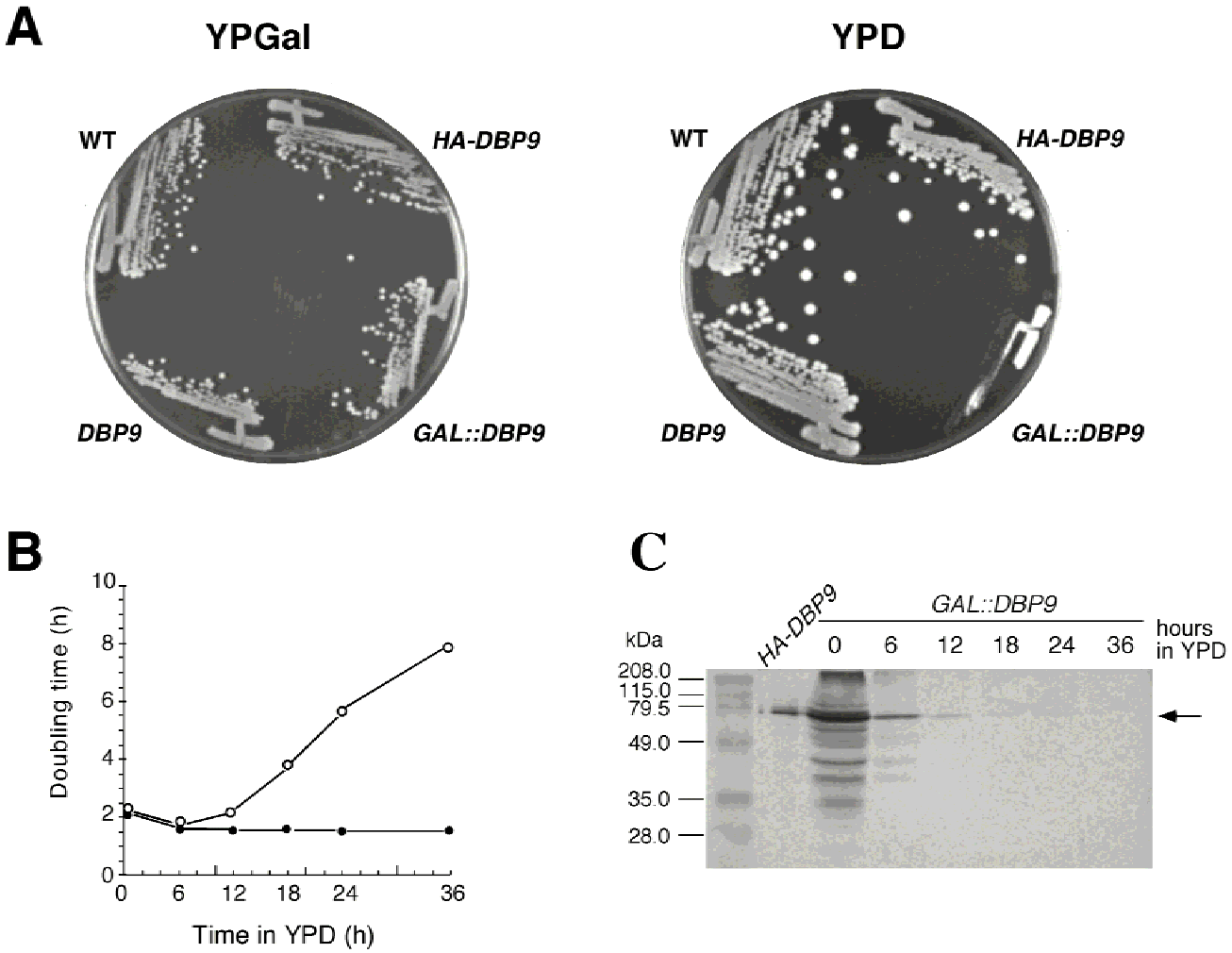

FIGURE 2. Growth of yeast cells is impaired upon Dbp9p depletion. **A:** Growth comparison of the strains MCD9H-2A (WT), MCD9H-2D YCplac33-*DBP9* (*DBP9*), MCD9H-2D YCplac111-*HA-DBP9* (*HA-DBP9*), and MCD9H-2D pAS24-*DBP9* (*GAL::DBP9*). Freshly grown cells were streaked on YPGal (galactose) and YPD (glucose) plates and incubated at 30 °C for 3 days. **B:** Growth curves of MCD9H-2D YCplac33-*DBP9* (*DBP9*; closed circles) and MCD9H-2D pAS24-*DBP9* (*GAL::DBP9*; open circles) at 30 °C after logarithmic cultures were shifted from YPGal to YPD medium for up to 36 h. Data are given as doubling times in YPD medium. **C:** Western blot analysis of HA-Dbp9p expressed from its cognate promoter and of the Dbp9p depletion. Whole-cell extracts of the strains MCD9H-2D YCplac111-*HA-DBP9* (*HA-DBP9*) and MCD9H-2D pAS24-*DBP9* (*GAL::DBP9*) were prepared from cells grown to logarithmic phase in YPD (for *HA-DBP9*) or from cells harvested at the indicated times after the shift to YPD medium (for *GAL::DBP9*). Equal amounts of protein were separated by 12.5% SDS-PAGE and HA-Dbp9p (indicated by an arrow) was detected by western blotting using monoclonal mouse anti-HA antibody 16B12 and goat anti-mouse alkaline phosphatase-conjugated antibodies. Prestained broad range molecular weight markers (Bio-Rad) were used as standards for molecular mass determination.

Dbp9p is predominantly localized in the nucleolus (Fig. 3D). Only a weak background staining was obtained with anti-HA antibodies on the control strain containing untagged Dbp9p (data not shown).

Dbp9p depletion leads to a 60S ribosomal subunit shortage and the formation of half-mer polysomes

The nucleolar localization of Dbp9p argues in favor of a participation of this protein in ribosome biogenesis. We therefore started the phenotypic characterization by polysome profile analysis to determine if the ribosome content of the cell was affected upon depletion of Dbp9p. For this purpose, the *GAL::DBP9* strain was grown at 30 °C in YPGal medium, shifted to YPD medium, and then polysome extracts were prepared from cells harvested 6 h, 12 h, and 18 h after the shift to nonpermissive conditions. Polysome profiles similar to those of a wild-type strain (data not shown) were obtained after 6 h (Fig. 4A); however, alterations in the profiles appeared after 12 h and became more pronounced after 18 h under nonpermissive conditions (Fig. 4B,C). The Dbp9p-depleted strain showed a def-

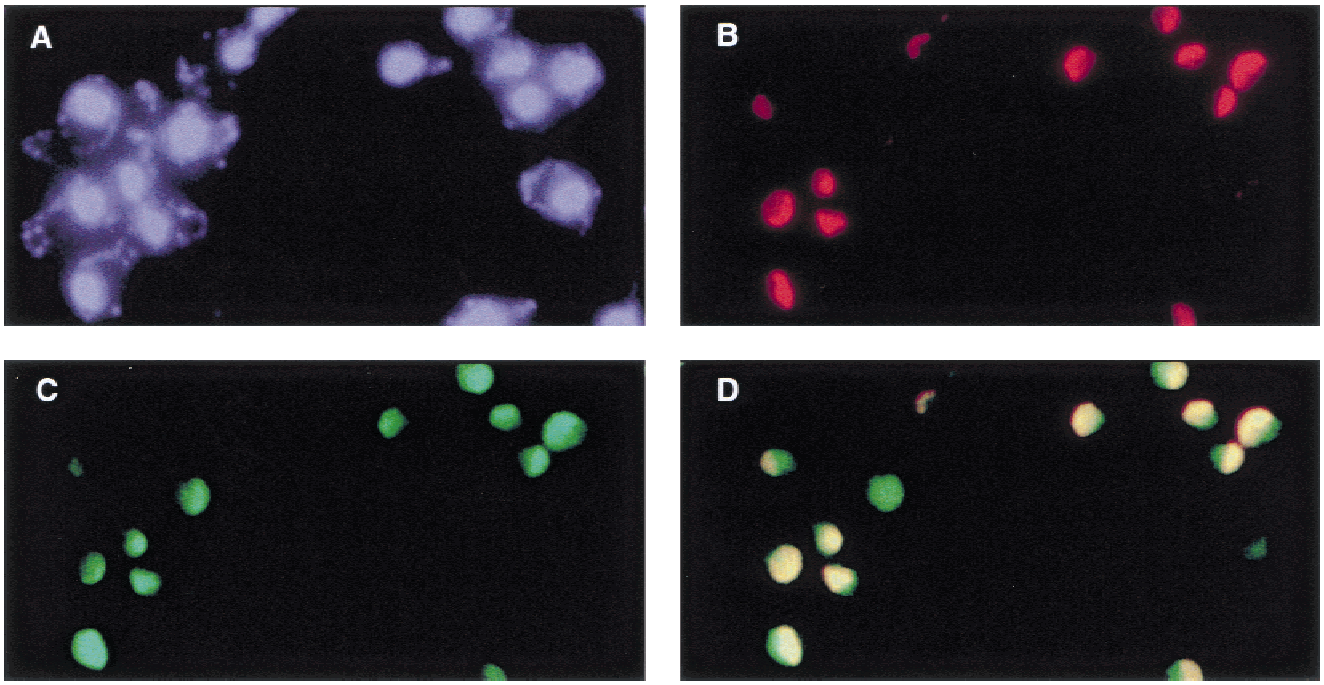

FIGURE 3. HA-Dbp9p localizes to the nucleolus. Indirect immunofluorescence was performed with cells expressing HA-Dbp9p from the *DBP9* promoter (MCD9H-2D YCplac111-*HA-DBP9*). **A:** DNA was stained with DAPI. **B:** The nucleolar marker protein Nop1p was detected with polyclonal rabbit anti-Nop1p antibodies, followed by decoration with goat anti-rabbit rhodamine-conjugated antibodies. **C:** HA-Dbp9p was detected with monoclonal mouse anti-HA antibody 16B12, followed by decoration with goat anti-mouse fluorescein-conjugated antibodies. **D:** Superimposition of the HA-Dbp9p and Nop1p signals.

icit of free 60S versus 40S ribosomal subunits, an overall decrease in 80S ribosomes (free couples and monosomes), and an accumulation of half-mer polysomes. The 60S ribosomal subunit shortage was confirmed by quantifying total ribosomal subunits in polysome run-off and low Mg^{2+} cell extracts. Six hours after the shift to YPD medium, the 60S to 40S ratio was about 1.8. The same ratio was obtained for the wild-type strain, whereas it dropped to 1.4 after 18 h of Dbp9p depletion. These results show that the cellular ribosome metabolism is affected by the absence of Dbp9p, which appears to play a role in the biogenesis of 60S ribosomal subunits.

Formation of 25S and 5.8S rRNAs is impaired upon Dbp9p depletion

To characterize the basis of the net deficit of 60S ribosomal subunits of the *GAL::DBP9* strain, we then analyzed the effect of Dbp9p depletion on the synthesis and processing of pre-rRNAs by [methyl-^{3}H] methionine pulse-chase labeling experiments. Wild-type and *GAL::DBP9* strains were pregrown as exponential cultures in YPGal and then transferred to SD-Met for 18 h ($OD_{600} \sim 0.8$). At this time point, the doubling time of the *GAL::DBP9* strain was around 5 h, compared to 2.5 h for the wild-type strain. Cells were pulse labeled for 1 min then chased for 2, 5, and 15 min with an excess of cold methionine. In the wild-type strain, the 35S precursor was rapidly converted into the 32S pre-rRNA and then into the 27S and 20S pre-rRNAs that were subsequently processed to the mature 25S and 18S rRNAs, respectively (Fig. 5A, lanes 1 to 4). Within the first minutes of chase, the radioactive 35S pre-rRNA was entirely processed and the labeled mature rRNAs reached their maximum levels after 5 min, when most of the labeled precursors had disappeared. In the *GAL::DBP9* strain, the processing of the 35S was delayed, part of it being still visible after 2 min of chase, and almost no 32S precursor was formed. The formation of 18S rRNA was slightly impaired as shown by the lower levels of the 20S precursor and the appearance of an aberrant 23S species (Fig. 5A, lanes 5 and 6). The formation of the 25S rRNA was more drastically affected as shown by the net decrease observed in the ratio of labeled 25S to 18S mature rRNAs (Fig. 5A, lanes 3–4 and 7–8). Much fewer 27S species were formed and the 27SB species did not persist until the 2-min chase point (Fig. 5A). This finding is consistent with a deficit in 60S ribosomal subunits, as observed by polysome analysis.

To exclude a defect in rRNA methylation and to monitor the processing and the formation of low molecular weight RNAs, pulse-chase labeling with [5,6-^{3}H]uracil was also performed. The wild-type and the *GAL::DBP9* strain, containing the plasmid YCplac33, were first grown

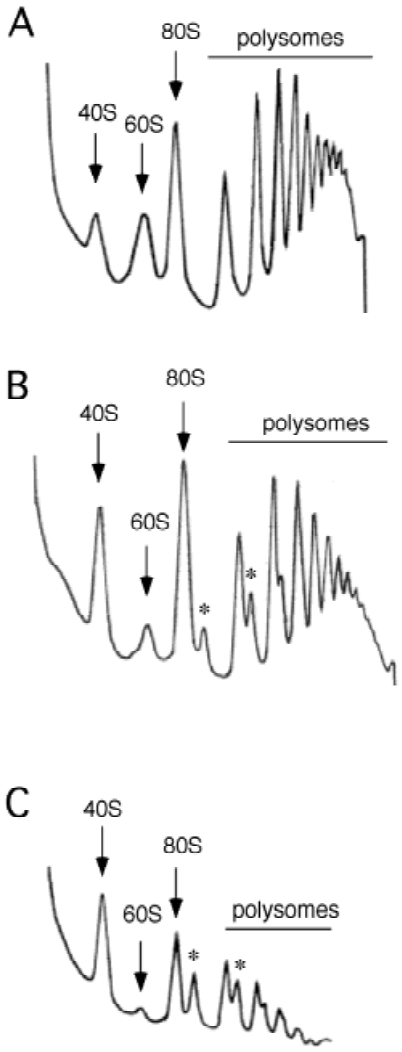

FIGURE 4. Depletion of Dbp9p results in a deficit in 60S ribosomal subunits, accumulation of half-mer polysomes, and an overall decrease in polysome content. The *GAL::DBP9* strain MCD9H-2D pAS24-*DBP9* was grown at 30 °C in YPGal medium and shifted to YPD medium for 6 (**A**), 12 (**B**), and 18 h (**C**). Cells were harvested at an OD_{600} of ~0.8 and similar amounts of cell extracts (12 A_{260} U) were resolved in 7–50% (w/v) sucrose gradients. Gradient analysis was performed with an ISCO UV-6 gradient collector with continuous monitoring at A_{254}. Sedimentation is from left to right. The peaks of free 40S and 60S ribosomal subunits, 80S free couples/monosomes, and polysomes are indicated. Half-mer polysomes are indicated by asterisks.

in SGal-Ura medium to exponential phase and then for 18 h in SD-Ura (OD_{600} ~1). At this time, the doubling time of the *GAL::DBP9* strain was increased by twofold compared to that of the wild-type strain. The cells were pulse labeled for 2 min and then chased for 5, 15, 30, and 60 min with an excess of cold uracil. Analysis of total RNA samples by agarose gel electrophoresis gave comparable results to the ones obtained by [methyl-^{3}H]methionine pulse-chase labeling (data not shown), although the conversion of pre-rRNAs to mature rRNA species was, as expected, kinetically slower for both the wild-type and the *GAL::DBP9* strain. Therefore, a global defect in rRNA methylation following Dbp9p depletion can be excluded. Analysis of low molecular weight RNAs by polyacrylamide gel electrophoresis showed that the synthesis of mature 5.8S rRNA was reduced upon Dbp9p depletion, whereas the synthesis of 5S rRNA was only mildly, if at all, affected (Fig. 5B). Moreover, labeling and processing of tRNAs was comparable in wild-type and Dbp9p-depleted cells.

To further define the pre-rRNA processing steps that are affected upon Dbp9p depletion, steady-state levels of pre- and mature rRNA species were determined by northern analyses. Different oligonucleotides hybridizing to defined regions of the 35S pre-rRNA transcript (see Fig. 1) were used to monitor specific processing intermediates in a wild-type control strain and during a time course of Dbp9p depletion. As seen in Figure 6A, depletion of Dbp9p resulted in a moderate decrease in 18S rRNA and a more drastic decrease in 25S rRNA steady-state levels. Probing with oligonucleotide B, which hybridizes 5′ to site A_0, revealed that the *GAL::DBP9* strain slightly accumulated, with ongoing depletion of Dbp9p, the 35S pre-rRNA and an aberrant 23S rRNA species (Fig. 6B). A signal corresponding to this rRNA species was obtained with probes C and D (Fig. 6C,D) but not with probe E (Fig. 6E), which shows that it extends from the 5′ end of the 35S precursor to site A_3 in ITS1 and indeed corresponds to the 23S rRNA. The mild accumulation of the 35S pre-rRNA and the 23S rRNA is in agreement with the [methyl-^{3}H]methionine pulse-chase labeling data and indicates that the early cleavages at sites A_0, A_1, and A_2 are at least delayed. Moreover, the amounts of the 32S pre-rRNA (Fig. 6C–F) and of the 20S precursor to mature 18S rRNA (Fig. 6C) diminished, and the steady-state levels of the $27SA_2$ pre-rRNA were drastically affected (Fig. 6D,E). Importantly, hybridization with oligonucleotide F, located between sites E and C_2, revealed a very dramatic depletion of the 27SB pre-rRNA species, which likely accounts for the net deficit in 60S-ribosomal-subunit levels.

To assess the steady-state levels of the 33S and the $27SA_3$ pre-rRNA species and to discriminate between the $27SB_L$ and $27SB_S$ precursors, we performed primer extension analysis. This analysis confirmed that Dbp9p depletion led to a net decrease of the $27SA_2$ precursor and of both 27SB pre-rRNAs (Fig. 7C), and it revealed that the steady-state levels of the $27SA_3$ pre-rRNA were also diminished (Fig. 7B). The levels of the 33S pre-rRNA were not affected, which is in agreement with cleavage at site A_0 being only kinetically delayed (Fig. 7A). Furthermore, primer extension showed that processing at all tested sites remained correct at the nucleotide level during the time course of Dbp9p depletion.

Altogether, our results indicate that the observed deficit in 60S ribosomal subunits is a consequence of the impaired formation of the 27S precursors, thus leading

to decreased steady-state levels of the mature 25S and 5.8S rRNAs. The above phenotypes are most likely due to the instability of an early pre-ribosomal particle upon depletion of Dbp9p.

Dbp9p functionally interacts with Dbp6p

While the phenotypic analysis of Dbp9p was in progress, we also isolated *DBP9* in an exhaustive multicopy suppressor screen as an exclusive dosage suppressor of the temperature-sensitive growth phenotype of the *dbp6-13* mutant at 35 °C (see Materials and Methods and Kressler et al., 1999a). Because increased dosage of *DBP9* only weakly suppressed the temperature sensitivity of the *dbp6-13* allele, we examined its suppressor activity at lower temperatures and we also tested for suppression of other *dbp6* alleles. By this analysis, we found that: (1) suppression of the *dbp6-13* allele was more pronounced at 30 °C than at 35 °C (data not shown); (2) both the slow-growth and the cold-sensitive phenotype of the *dbp6-4* allele were very efficiently suppressed (Fig. 8A and data not shown); (3) *CEN* and *2μ*-borne *DBP9* suppressed almost equally well the *dbp6-4* mutation at both 30 and 18 °C (Fig. 8A and data not shown); and (4) increased dosage of *DBP9* did not suppress the temperature-sensitive *dbp6-2*, *-3* and *-10* alleles at 37 °C (data not shown). We confirmed the solid-medium suppression by comparing the growth rates of a *dbp6-4* mutant strain (YDK8-1A pRS415-*dbp6-4*) that was either transformed with pRS414-*HA-DBP6*, YCplac22-*HA-DBP9*, YEplac112-*HA-DBP9,* or the empty vector YCplac22 in liquid SD-Trp medium at 30 °C. Doubling times of *dbp6-4* harboring strains at 30 °C were 1.65, 2.4, 2.2, and 3.7 h for the complemented, low-copy suppressed, high-copy suppressed, or nonsuppressed *dbp6-4* mutant strains, respectively. To test whether the efficient suppression of the growth phenotype was due to restoration of the 60S-ribosomal-subunit deficiency, we subjected cell extracts of the above strains, which were grown at 30 °C, to polysome analysis. The profile of the *dbp6-4* mutant strain was, as expected, typical of a mutant affected in 60S-ribosomal-subunit biogenesis, as evidenced by a strong reduction in the level of free 60S ribosomal subunits, appearance of half-mer polysomes, and an overall decrease in polysome content (Fig. 8B). Complementation of the growth defect by plasmidic *DBP6* resulted in wild-type polysome profiles (Fig. 8C). Introduction of either monocopy, although to a slightly lesser extent, or multicopy *DBP9* led to an increase in the levels of free 60S ribosomal subunits, an almost complete disappearance of half-mer polysomes, and a substantial increase in overall polysome content (data not shown and Fig. 8D). We conclude that *DBP9* is a very efficient dosage suppressor of the slow-growth phenotype of

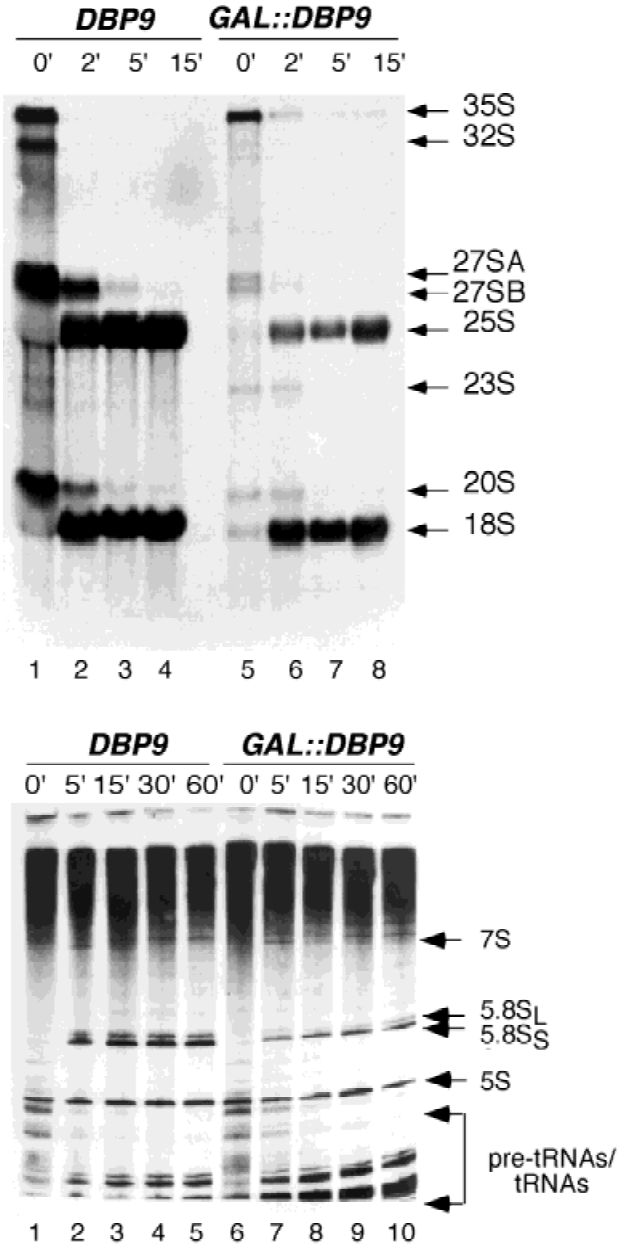

FIGURE 5. Dbp9p depletion leads to reduced formation of the 27S pre-rRNAs and thus of the mature 25S and 5.8S rRNAs. **A:** Strains MCD9H-2D YCplac33-*DBP9* (*DBP9*) and MCD9H-2D pAS24-*DBP9* (*GAL::DBP9*) were grown at 30 °C in YPGal medium and shifted to SD-Met medium for 18 h (OD_{600} ~0.8). Cells were pulse-labeled for 1 min with [methyl-^{3}H]methionine and then chased for 2, 5, and 15 min with an excess of cold methionine. Total RNA was extracted, and 20,000 cpm were loaded and separated on a 1.2% agarose-formaldehyde gel, transferred to a nylon membrane, and visualized by fluorography. **B:** Strains MCD9H-2D YCplac33-*DBP9* (*DBP9*) and MCD9H-2D pAS24-*DBP9* YCplac33 (*GAL::DBP9*) were grown at 30 °C in SGal-Ura medium and shifted to SD-Ura medium for 18 h (OD_{600} ~1). Cells were pulse labeled for 2 min with [5,6-^{3}H]uracil and then chased for 5, 15, 30, and 60 min with an excess of cold uracil. Total RNA was extracted, and 30,000 cpm were loaded and separated on a 7% polyacrylamide-8 M urea gel, transferred to a nylon membrane, and visualized by fluorography. The positions of the different pre-rRNAs, mature rRNAs, and tRNAs are indicated.

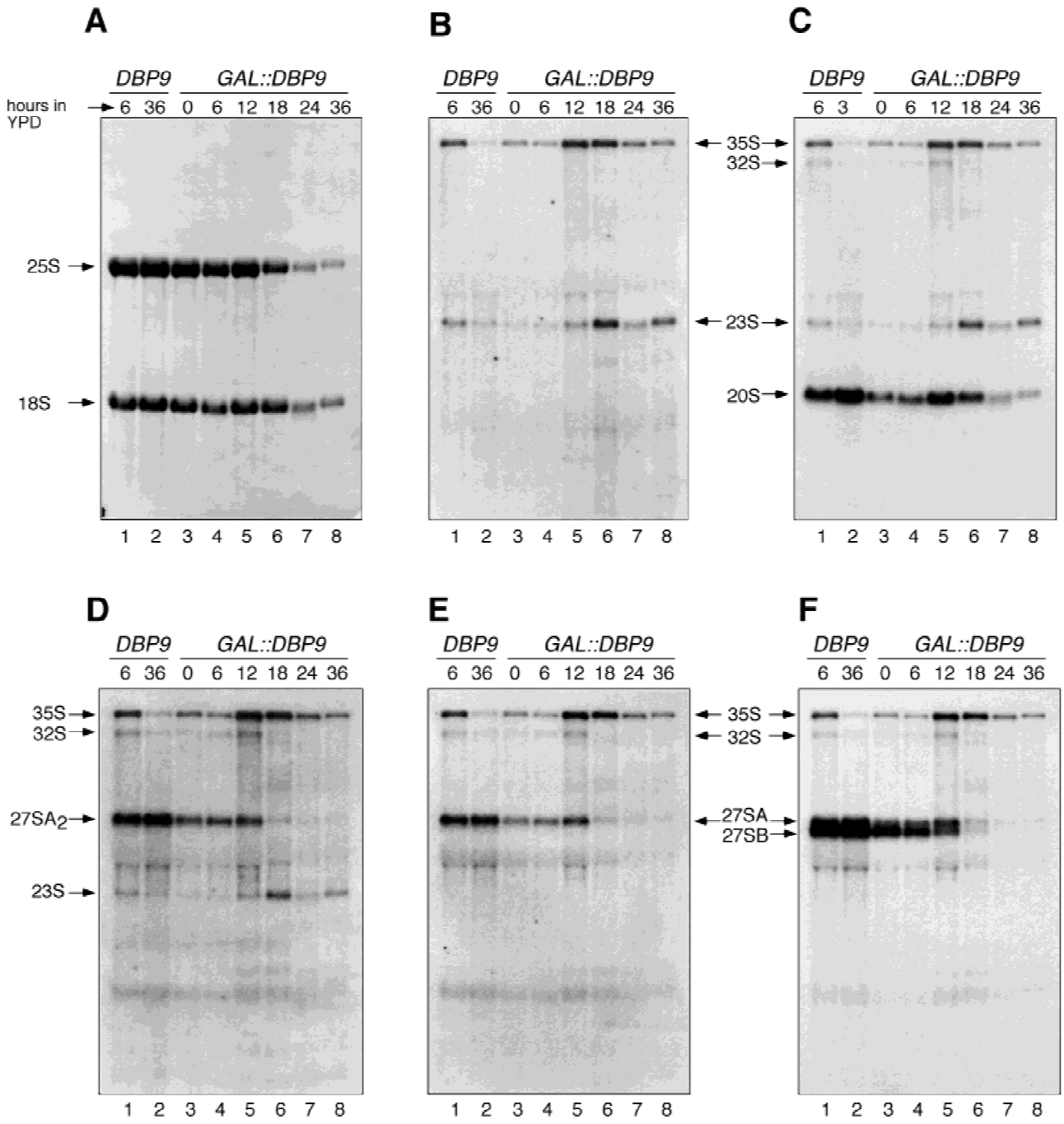

FIGURE 6. Depletion of Dbp9p strongly affects the steady-state levels of the 27S pre-rRNAs and leads to a deficit in mature 25S rRNA. Strains MCD9H-2D YCplac33-*DBP9* (*DBP9*) and MCD9H-2D pAS24-*DBP9* (*GAL::DBP9*) were grown in YPGal medium and then shifted to YPD medium. Cells were harvested at the indicated times and total RNAs were extracted. Equal amounts of total RNA (5 μg) were resolved on a 1.2% agarose-formaldehyde gel and transferred to a nylon membrane. The membrane was stained with methylene blue (**A**) and then consecutively hybridized with the different probes indicated in Figure 1. **B:** Oligonucleotide B 5′ of site A_0; **C:** oligonucleotide C in ITS1 between sites D and A_2; **D:** oligonucleotide D in ITS1 between sites A_2 and A_3; **E:** oligonucleotide E in ITS1 3′ of site A_3; **F:** oligonucleotide F in ITS2 between sites E and C_2. The positions of the different pre-rRNAs and mature rRNAs are indicated.

the *dbp6-4* allele. Furthermore, this suppression can be fully explained at a molecular level by the almost complete restoration of the synthesis of 60S ribosomal subunits.

To complement the above finding, we extended the genetic interaction analysis to assessing the growth phenotypes of *dbp6/dbp9* double mutant strains (see Materials and Methods). As shown in Figure 9A,B, the

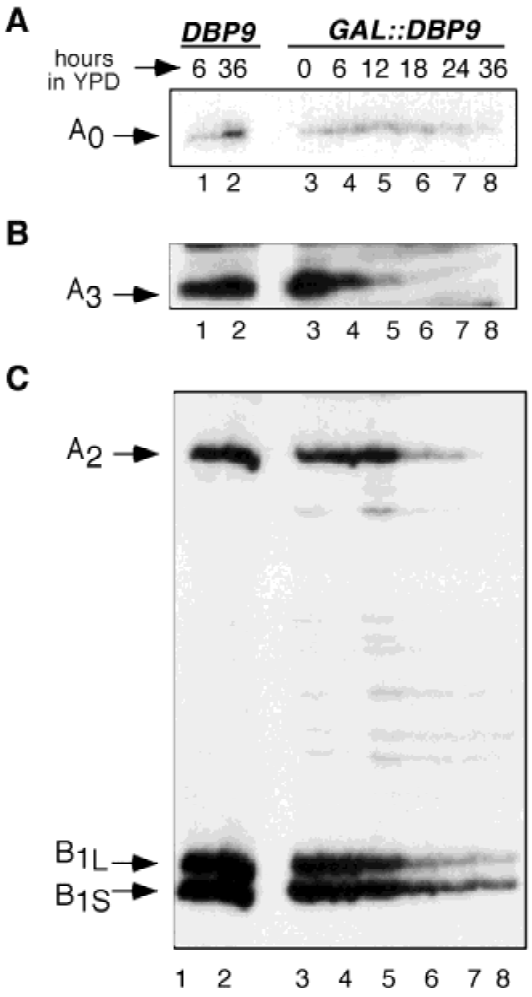

FIGURE 7. Primer extension analysis of the 27S pre-rRNAs and the 33S precursor. The same samples of total RNA as in Figure 6 were used. **A:** Primer extension through 5′ ETS was performed using oligonucleotide I and allows detection of the 33S pre-rRNA (site A_0). **B:** Primer extension using oligonucleotide E in ITS1 allows detection of the $27SA_3$ pre-rRNA (site A_3). **C:** Primer extension with oligonucleotide G in ITS2, between sites C_1 and C_2, reveals processing sites A_2, B_{1L}, and B_{1S}, allowing detection of the $27SB_L$ and $27SB_S$ pre-rRNA species. The primer extension stops corresponding to the different pre-RNA species are indicated by arrows.

combination of *dbp9* mutations with mild *dbp6* alleles led to a strong synthetic enhancement of the respective phenotypes. Moreover, and in agreement with previous synthetic interaction analyses (Kressler et al., 1999a), no viable *dbp9/dbp6-4* or *dbp9/dbp6-13* double mutants could be recovered (see Materials and Methods), indicating that *dbp9* alleles were synthetically lethal with the strong *dbp6-4* and *dbp6-13* alleles.

We have previously shown that mutations in the two putative RNA helicase encoding genes *DBP6* and *DBP7* show a synthetic enhancement of their mutant phenotypes (Daugeron & Linder, 1998). To test whether mutations in *DBP9* are synthetically enhanced by a *dbp7* null allele, we tested growth of the *dbp9-1* allele in presence and absence of a functional *DBP7* gene. Although a *dbp7* null allele already confers a severe slow growth phenotype, introduction of a *dbp9-1* allele synthetically enhances the mutant phenotype even more (data not shown). In contrast, a combination of the *spb4-1* and the *dbp9-1* allele does not show any synthetic enhancement (data not shown). This clearly demonstrates that the genetic interactions described above are specific and not solely due to an implication in the same cellular process, that is, 60S ribosome biogenesis.

The two putative RNA helicases Dbp9p and Dbp6p interact in a yeast two-hybrid assay

Because *DBP6* and *DBP9* functionally interacted in two different genetic tests, we next asked whether Dbp6p and Dbp9p also physically interacted. For this purpose, we cloned *DBP6* and *DBP9* into the yeast two-hybrid vectors pACTII and pAS2ΔΔ (Materials and Methods), transformed these constructs with the appropriate control plasmids into the reporter strain PJ69-4A (James et al., 1996), and tested the transformants for growth on SD-Trp-Leu-His plates. Interestingly, the combinations of the AD-*DBP6*/BD-*DBP6*, AD-*DBP9*/BD-*DBP6,* and AD-*DBP9*/BD-*DBP9* plasmids allowed for growth of the reporter strain on minimal medium lacking histidine (Fig. 10); however, growth was no longer supported when as little as 1 mM 3-amino-triazole (3-AT) was added to the medium (data not shown). Thus, the above combinations of AD- and BD-fusions bring the GAL4 DNA-BD and GAL4 AD into close enough proximity for low-level *HIS3* reporter transcriptional activation to occur, which suggests that Dbp6p and Dbp9p both very weakly interact with themselves and with each other (see the Discussion). The finding that the combination of the AD-*DBP6* and BD-*DBP9* constructs did not allow for growth on medium lacking histidine indicates that different domains within the two proteins may be responsible for homo- and heteromerization, because the same constructs allowed for growth in the absence of histidine if assessed together with their respective homo-partners. Moreover, there probably is, in contrast to the AD-*DBP9*/BD-*DBP6* combination, a steric hindrance to the interaction between AD-Dbp6p and BD-Dbp9p. To confirm the specificity of these weak interactions, we also tested the *DBP6* and *DBP9* constructs in combination with *FAL1* and *SPB4* two-hybrid constructs. Fal1p and Spb4p are two DEAD-box proteins that are involved in 40S- and 60S-ribosomal-subunit biogenesis, respectively (Kressler et al., 1997; de la Cruz et al., 1998). These functionally unrelated DEAD-box proteins did neither interact with themselves nor with the Dbp6p and Dbp9p fusion proteins (data not shown).

In conclusion, the above genetic and two-hybrid data, together with the similar phenotypes observed upon Dbp6p or Dbp9p depletion, strongly argue in favor of a

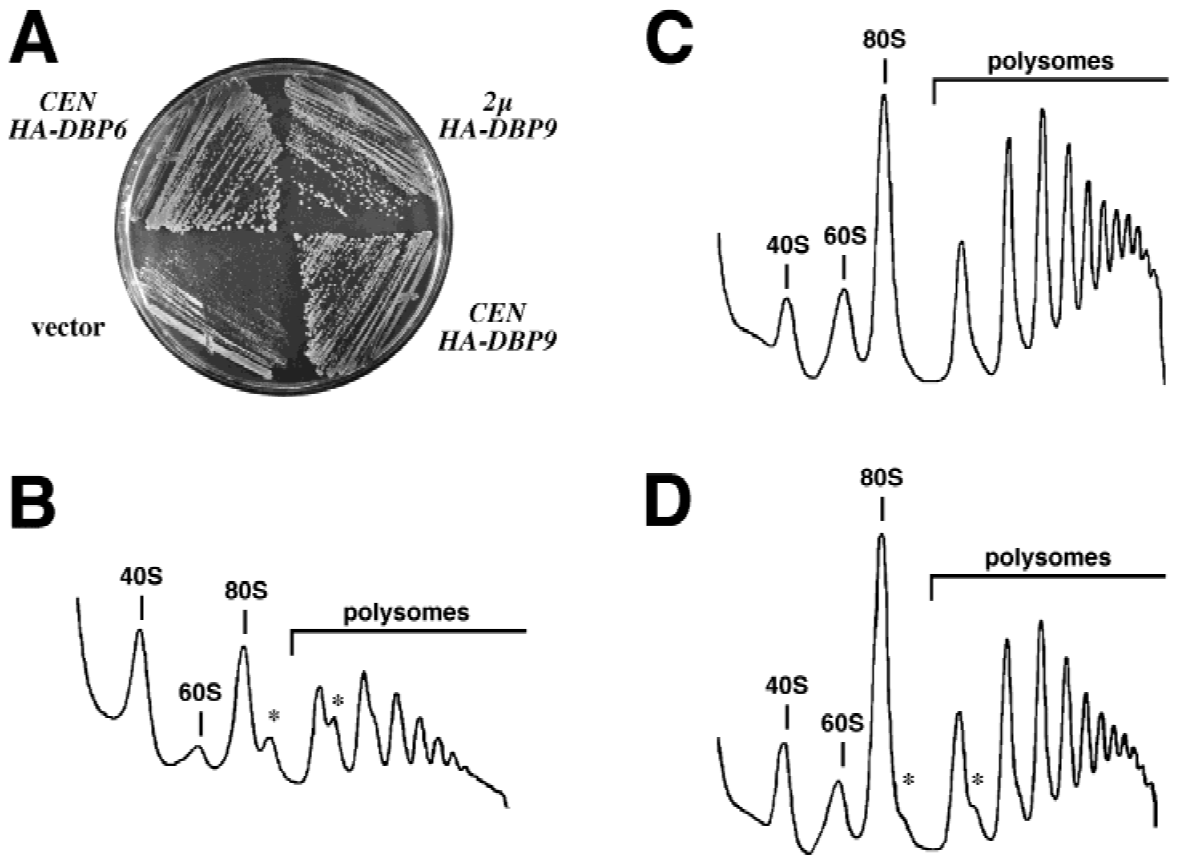

FIGURE 8. *DBP9* is a dosage suppressor of *dbp6* alleles. YDK8-1A pRS415-*dbp6-4* was transformed with pRS414-*HA-DBP6* (*CEN-HA-DBP6*), YCplac22-*HA-DBP9* (*CEN-HA-DBP9*), YEplac112-*HA-DBP9* (*2μ-HA-DBP9*), and empty vector (vector). **A:** Representative transformants are shown on a SD-Trp plate that was incubated for 48 h at 30 °C. Transformants *dbp6-4* (empty vector) (**B**), complemented *dbp6-4* mutant (*CEN-HA-DBP6*) (**C**), and suppressed *dbp6-4* mutant (*2μ-HA-DBP9*) (**D**), were grown in liquid SD-Trp at 30 °C and harvested at an OD_{600} between 0.4 and 0.8. Cell extracts were resolved in 7–50% sucrose gradients. Gradients were analyzed by continuous monitoring at A_{254}. Sedimentation is shown from left to right. The peaks of free 40S and 60S subunits, 80S ribosomes (free couples and monosomes), and polysomes are indicated. Half-mers are indicated by asterisks.

functional interaction between Dbp6p and Dbp9p in the process of 60S-ribosomal-subunit assembly.

DISCUSSION

Sequence similarity searches using Dbp9p reveal several highly conserved proteins from different organisms, including humans. The human homolog, NOH61, has been shown to reside predominantly in the nucleolus (Zirwes et al., 2000), as we have shown here for Dbp9p. Although the C-terminal parts of the two proteins are highly similar, the predicted nuclear localization signals present in NOH61 are not conserved in Dbp9p. However, because the C-terminal extensions are rich in lysines and arginines, other noncanonical nuclear localization signal sequences could mediate nuclear import of Dbp9p. Interestingly, NOH61 cannot functionally replace Dbp9p, because its heterologous expression in yeast did not complement the absence of Dbp9p (data not shown).

Recombinant NOH61 has been shown to exhibit nucleic acid-stimulated ATPase activity (Zirwes et al., 2000); however, further experiments are required to determine the precise in vitro activities of either NOH61 or Dbp9p. Our yeast two-hybrid data raise the possibility that Dbp9p, as well as Dbp6p, have the potential to weakly interact with themselves. At least in the case of Dbp9p, our data are corroborated by the finding that in vitro-translated NOH61 (predicted molecular mass of 61 kDa) peaks, at a salt concentration of 100 mM NaCl, in sucrose gradients or upon gel-filtration chromatography at an apparent molecular mass of 300 kDa (Zirwes et al., 2000). Even though highly speculative, the ability of these proteins to form homo-oligomeric complexes may be mechanistically relevant for their ATPase or potential "helicase" activities (Bird et al., 1998).

When Zirwes et al. (2000) performed fractionation of *Xenopus* oocyte nuclei, the majority of NOH61 was found in the low-speed pellet containing nucleoli, nu-

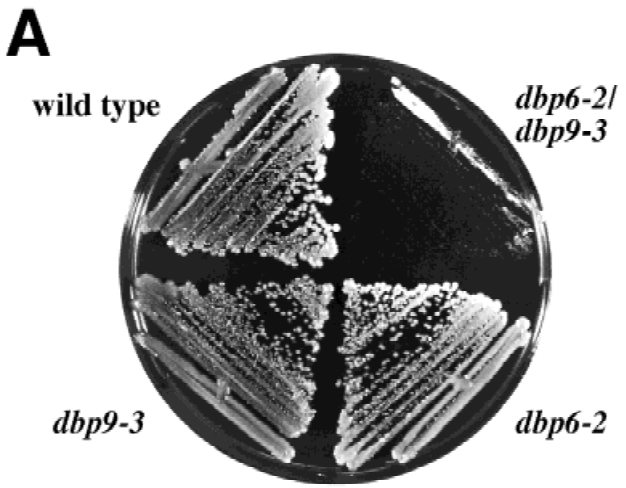

B

	dbp9-1 2.1 h	*dbp9-3* 1.6 h	*dbp9-5* 3.15 h
dbp6-2 2 h	6.9 h	5 h	8.5 h
dbp6-3 1.95 h	9.1 h	6.75 h	12 h

FIGURE 9. Mild *dbp6* alleles strongly synthetically enhance the moderate growth defect of *dbp9* mutants. **A:** Wild-type, *dbp9-3*, *dbp6-2*, and *dbp6-2/dbp9-3* strains are shown on a YPD plate that was incubated for 48 h at 30 °C. **B:** *dbp6* and *dbp9* single mutants as well as the different *dbp6/dbp9* double mutant combinations were grown in liquid YPD medium at 30 °C for measurement of the respective doubling times. A doubling time of 1.4 h was obtained for the wild-type control strain.

clear envelopes, and chromosomes. However, a significant amount of NOH61 was still present in the high-speed pellet (HSP) fraction, which is highly enriched in free nucleoplasmic pre-ribosomal particles (Hügle et al., 1985). By subjecting the HSP fraction, after resolubilization in a 100-mM NaCl-containing buffer, to sucrose gradient fractionation, they revealed that NOH61 was specifically associated with 65S pre-ribosomal particles (Zirwes et al., 2000). Moreover, NOH61 was found to be significantly enriched in the granular component of HeLa cell nucleoli (Zirwes et al., 2000), which is made up of nearly completed pre-ribosomal particles (Olson et al., 2000). Altogether, these findings led Schmidt-Zachmann and coworkers to postulate that NOH61 may have a role in later stages of the processing of the pre-ribosomal particles leading to mature 60S ribosomal subunits (Zirwes et al., 2000).

The results presented in this study, however, support a model where Dbp9p would act at a very early step in the formation of 60S ribosomal subunits. First, the most pronounced pre-rRNA processing phenotype associated with the genetic depletion of Dbp9p is the reduced formation and the lower steady-state levels of all 27S precursors, especially of the 27SB pre-rRNAs, to mature 25S and 5.8S rRNA. Similar phenotypes have been observed upon depletion of other protein *trans*-acting factors (Bergès et al., 1994; Sun & Woolford, 1994; Kressler et al., 1998; Zanchin & Goldfarb, 1999), and they are most readily explained by the instability of early pre-ribosomal particles (discussed in Kressler et al., 1999b). Second, Dbp9p depletion affects 18S rRNA production more drastically than depletion of other protein *trans*-acting factors involved in 60S-ribosomal-subunit biogenesis does (Bergès et al., 1994; Sun & Woolford, 1994; de la Cruz et al., 1998; Kressler et al., 1999c; Zanchin & Goldfarb, 1999; Burger et al., 2000). Intriguingly, the block of the early cleavages at sites A_0 to A_2, however, seems to be less pronounced, as judged by the relatively low levels of 23S rRNA accumulation, upon Dbp9p depletion. One conceivable explanation is that the instability of early pre-ribosomal particles is masking the effect of inhibited A_0 to A_2 cleavage; delayed or blocked cleavage at these sites is generally observed in mutants affecting 60S-ribosomal-subunit biogenesis (discussed in Venema & Tollervey, 1999). Finally, our genetic data (synthetic lethality, dosage suppression, and weak interaction in a yeast two-hybrid assay) indicate that Dbp9p functionally interacts with Dbp6p, which has been previously suggested to be acting at an early step on the pathway to formation of 60S ribosomal subunits (Kressler et al., 1998, 1999a). The observed genetic interactions are highly specific because neither the *dbp9* nor *dbp6* mutant phenotypes are synthetically enhanced by, for example, the *spb4-1* mutation (data not shown and Kressler et al., 1999a). Moreover, the cold sensitivity of the *dbp6-4* mutant cannot be suppressed by overexpression of other DEAD-box proteins, such as Dbp10p and Spb4p, implicated in the biogenesis of 60S ribosomal subunits (data not shown).

Interestingly, this is the first time that a putative RNA helicase has been shown to suppress a mutation in another helicase gene involved in ribosome biogenesis. A similar suppression has so far only been demonstrated for the cytoplasmic Ded1p by its homolog Dbp1p (Jamieson & Beggs, 1991). However, in this case, overexpression of Dbp1p results in a bypass suppression, which is clearly not the case for the couple *DBP6*/*DBP9*. Increased dosage of Dbp9p allows suppression of certain *dbp6* mutant alleles indicating that Dbp9p directly or indirectly helps the mutated Dbp6 protein to exert its role. One possibility to explain a direct suppression would be the formation of heterodimers or -oligomers, as suggested by our yeast two-hybrid data. In this case, the nonfunctional Dbp6p homodimer would be replaced by a partially functional

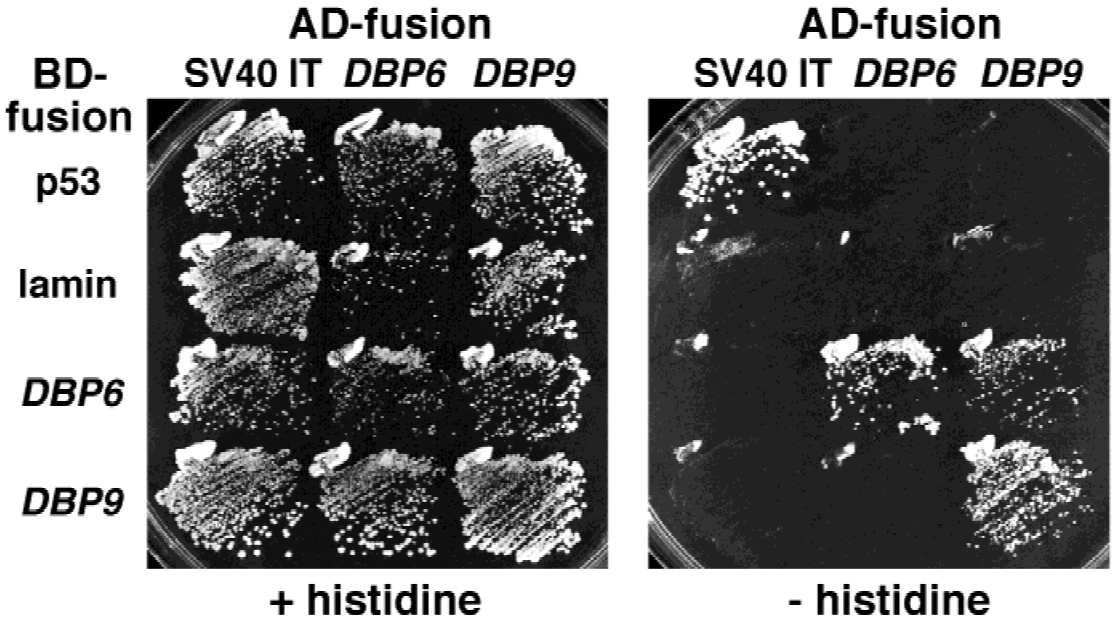

FIGURE 10. Yeast two-hybrid interaction analysis: Dbp6p and Dbp9p both very weakly interact with themselves and with each other. The two-hybrid reporter strain PJ69-4A was cotransformed with combinations of the GAL4 DNA-BD fusion plasmids pVA3-1 (p53), pLAM5′-1 (lamin), pAS2ΔΔ-*DBP6*, and pAS2ΔΔ-*DBP9* and the GAL4 AD fusion plasmids pTD1-1 (SV40 lT), pACTII-*DBP6*, and pACTII-*DBP9*. Transformants were selected on SD-Trp-Leu plates and then restreaked on SD-Trp-Leu (left panel) and on SD-Trp-Leu-His (right panel) plates that were incubated for 72 h at 30 °C. The SV40 lT AD-fusion combined with the p53 BD-fusion serves as the positive control and the SV40 lT AD-fusion combined with the lamin BD-fusion serves as the negative control. Combinations of the SV40 lT AD-fusion as well as of the p53 and the lamin BD-fusion plasmids with the respective *DBP6* and *DBP9* BD- and AD-fusion plasmids do not, as expected, allow for growth on SD-Trp-Leu-His plates, and are thus also regarded as negative controls.

Dbp6p/Dbp9p heterodimer, where the Dbp6p moiety confers the specificity and Dbp9p the main enzymatic activity. This would also explain why overexpression of Dbp9p cannot complement the *dbp6* null allele. However, due to the weakness of the two-hybrid interaction, we cannot rule out the possibility that the interaction between Dbp6p and Dbp9p is bridged via other proteins and pre-rRNAs within a pre-ribosomal particle. There are obviously other, more traditional, explanations for the observed dosage suppression. Assuming that both Dbp6p and Dbp9p are involved in rearranging pre-ribosomal particles, then the suppression could be explained by Dbp9p's increased efficiency to catalyze the Dbp9p-dependent structural rearrangements. If Dbp6p acts at a previous step, then the equilibrium would be shifted to the product of the Dbp6p-dependent structural rearrangement through the increased removal of the product by the strengthened Dbp9p activity.

What could be the substrates of Dbp6p and Dbp9p? As has been pointed out by Venema and Tollervey (1999), the many snoRNA–rRNA interactions need to be separated to allow mutually exclusive rRNA–rRNA and protein–rRNA interactions to occur. So far only the putative RNA helicases Rok1p, Dbp4p, and Dhr1p have been shown to interact genetically or physically with snoRNAs (Liang et al., 1997; Venema et al., 1997; Colley et al., 2000). However, there are by far many more snoRNA–rRNA base pairings than there are putative RNA helicases (Venema & Tollervey, 1999). Yet, another potential function for putative RNA helicases during ribosome biogenesis, besides the rearrangement of inter- and intramolecular (pre-)rRNA interactions, might be the dissociation of proteins from (pre-)rRNA. Such an activity can be postulated based on recent biochemical and genetic evidence. Jankowsky et al. (2001) demonstrated an in vitro protein–RNA dissociating activity of the viral helicase NPH-II using an artificial substrate. In accordance with such an activity, two recent publications reported genetic data on a putative protein–RNA dissociating activity of DEAD-box proteins (for reviews, see Linder et al., 2001; Schwer, 2001). Kistler and Guthrie (2001) showed that deletion of the Mud2 protein, which binds to the intron of pre-mRNA, renders the putative RNA helicase Sub2p dispensable. Similarly, Chen et al. (2001) could show that a mutation in the U1-C protein or distinct mutations within the U1 snRNA can bypass the requirement of the putative RNA helicase Prp28p. Finally, it cannot formally be excluded that members of the DEAD-box protein family are involved in dissociation of protein–protein interactions in the context of a ribonucleoprotein particle. Thus, at present, a major challenge is to define the target structures of these putative RNA helicases. In the absence of an in vitro reconstitution system, the genetic ap-

TABLE 1. Yeast strains used in this study.

Name	Relevant genotype	Reference
W303	*MAT***a**/*MATα ura3-1/ura3-1 ade2-1/ade2-1 his3-11,15/his3-11, 15 leu2-3,112/leu2-3,112 trp1-1/trp1-1*	Thomas and Rothstein, 1989
MCD9H*	*DBP9/dbp9*::HIS3MX6	This study
MCD9H-2A[a]	*MATα DBP9*	This study
MCD9H-2D[b]	*MATα dbp9*::HIS3MX6 [YCplac33-*DBP9*]	This study
MCD9H-4C[b]	*MAT***a** *dbp9*::HIS3MX6 [YCplac33-*DBP9*]	This study
YDK9-2C	*MATα dbp6*::HIS3MX6 [pRS416-*dbp6-13*]	Kressler et al., 1999a
YDK9-2D	*MAT***a** *dbp6*::HIS3MX6 [pRS416-*dbp6-13*]	Kressler et al., 1999a
YDK8-1A	*MATα dbp6*::kanMX4 [pRS416-*DBP6*]	Kressler et al., 1998
YDK33	*dbp6*::kanMX4/*DBP6 dbp9*::HIS3MX6/*DBP9* [pRS416-*DBP6*; YCplac111-*HA-dbp9-1*]	This study
YDK34	*dbp6*::kanMX4/*DBP6 dbp9*::HIS3MX6/*DBP9* [pRS416-*DBP6*; YCplac111-*HA-dbp9-3*]	This study
YDK36	*dbp6*::kanMX4/*DBP6 dbp9*::HIS3MX6/*DBP9* [pRS416-*DBP6*; YCplac111-*HA-dbp9-5*]	This study
YDK33-8C	*MAT***a** *dbp6*::kanMX4 *dbp9*::HIS3MX6 [pRS416-DBP6; YCplac111-*HA-dbp9-1*]	This study
YDK34-4C	*MATα dbp6*::kanMX4 *dbp9*::HIS3MX6 [pRS416-*DBP6*; YCplac111-*HA-dbp9-3*]	This study
YDK36-26C	*MAT***a** *dbp6*::kanMX4 *dbp9*::HIS3MX6 [pRS416-*DBP6*; YCplac111-*HA-dbp9-5*]	This study
PJ69-4A	*MAT***a** *trp1-901 leu2-3,112 ura3-52 his3-200 gal4Δ gal80Δ LYS2*::*GAL1-HIS3 GAL2-ADE2 met2*::*GAL7-lacZ*	James et al., 1996

*All strains are derivatives of W303 except when indicated.
[a]Wild-type meiotic segregant of MCD9H.
[b]Δ*dbp9* meiotic segregant of MCD9H requiring a plasmid-borne *DBP9* allele to support growth. Depending on the experimental conditions and as indicated in the text, the original plasmid YCplac33-*DBP9* was replaced by other *DBP9*-containing plasmids.

proach will be essential in elucidating the functional environments of the DEAD-box and related proteins.

MATERIALS AND METHODS

Strains, oligonucleotides, media, and microbiological methods

Yeast strains used in this study are described in Table 1, and oligonucleotides are listed in Table 2. Genetic manipulations and preparation of media were according to established procedures (Lundblad, 1994; Kaiser et al., 1994). Yeast cells were transformed using the lithium acetate method (Gietz et al., 1992). *Escherichia coli* DH10B was used for all recombinant DNA techniques (Sambrook et al., 1989). Tetrad dissections were performed using a Singer MS manual micromanipulator.

Plasmids

YCplac22-*HA-DBP9* (pDK443) and YEplac112-*HA-DBP9* (pDK444) were constructed by cloning an ~4-kb *Sal*I/*Sac*I-fragment from YCplac111-*HA-DBP9* (pMCD9-4) into the *Sal*I/*Sac*I-restricted vectors YCplac22 and YEplac112, respectively (Gietz & Sugino, 1988). Functionality of the above plasmids was confirmed by complementation of the *dbp9* null allele at 18, 30, and 37 °C. Expression levels were tested by western

TABLE 2. Oligonucleotides used in this study.

Name	Sequence (5′ to 3′)	Remarks
DBP9-P1	ATAGACTAAGCCAAAACTGCAACGAAAGATCAAAAAAATGCGTACGCTGCAGGTCGAC	SFH-PCR disruption of *DBP9*
DBP9-P2	GATTTTTACATAAAATATAGAATAAATATCAATATTATTAATCAATCGATGAATTCGAGCTCG	SFH-PCR disruption of *DBP9*
DBP9-G1	GGGGCCCCGTCGACAGCTATGAGAAAAAGTCG	*GAL*::*DBP9*
DBP9-G2	GGGGCCCCGCATGCCTATTCTTAAGAGGTGATTC	*GAL*::*DBP9*
DBP9-P3	AGTTTCAATTACAGGAATGAGG	*HA-DBP9*
DBP9-P4	GACTATGCGGGCTATCCCTATGACGTCCCGGACTATGCAAGCTATGAGAAAAAGTCTGTGG	*HA-DBP9*
DBP9-P5	GTCATAGGGATAGCCCGCATAGTCAGGAACATCGTATGGGTAGGATCCTGCCATTTTTTTG ATCTTTCGTTGCAG	*HA-DBP9*
Primer I	CCAGATAACTATCTTAAAAGAAGAAGC	Primer extension

blotting using the mouse monoclonal anti-HA antibody 16B12 (BAbCo). The plasmid pRS416-*dbp6-13* (pDK316) was constructed by cloning a 2.82-kb *Xho*I/*Sac*I-fragment from pRS415-*dbp6-13* (Kressler et al., 1999a) into the *Xho*I/*Sac*I-restricted vector pRS416 (Sikorski & Hieter, 1989). The plasmids pRS414-*dbp6-2*, pRS414-*dbp6-3*, pRS414-*dbp6-4*, pRS415-*dbp6-4*, pRS414-*dbp6-13*, and pRS414-*HA-DBP6* have been previously described (Kressler et al., 1999a).

Disruption and cloning of the *DBP9* gene

A HIS3MX6 marker cassette with short flanking *DBP9* homology regions was synthesized by PCR (SFH-PCR) using *Pfu* polymerase (Stratagene), the plasmid pFA6a-HIS3MX6 as the template, and the primer couple DBP9-P1 and DBP9-P2 (Wach et al., 1994). After concentration by ethanol precipitation, the SFH-PCR *dbp9*::HIS3MX6 product was transformed into the diploid strain W303 to substitute the entire *DBP9* coding sequence by homologous recombination. Transformants were selected on SD-His plates. The correct integration of the HIS3MX6 marker at the *DBP9* genomic locus resulted in the heterozygous diploid strain MCD9H (*DBP9*/*dbp9*::HIS3MX6). MCD9H was further subjected to sporulation and tetrad analysis.

The cognate *DBP9* gene was cloned from the cosmid 9328 (Chromosome XII) purchased from ATCC. Briefly, after complete digestion of the cosmid with *Sac*I, a 4.56-kb fragment was gel purified (Gene Clean™, BIO101, Inc.) and further digested with *Bgl*II. A 3.91-kb *Sac*I/*Bgl*II fragment containing *DBP9* was gel purified and subcloned into the *Sac*I/*Bam*HI-restricted plasmid YCplac33 (Gietz & Sugino, 1988) yielding the plasmid YCplac33-*DBP9* (pMCD9-1). The haploid strain MCD9H-2D [YCplac33-*DBP9*] (Δ*dbp9*) was obtained after sporulation and tetrad dissection of MCD9H transformed with YCplac33-*DBP9*. MCD9H-2D [YCplac33-*DBP9*] exhibited a wild-type growth behavior in all the tested conditions confirming that the plasmid-borne *DBP9* allele fully complemented the *dbp9*-null allele. A *Sac*I/*Pst*I insert from YCplac33-*DBP9* containing *DBP9* was further subcloned into the *Sac*I/*Pst*I-restricted plasmids YCplac111 and YEplac181 yielding plasmids YCplac111-*DBP9* (pMCD9-2) and YEplac181-*DBP9* (pMCD9-3), respectively.

Construction of the *GAL::DBP9* allele and in vivo depletion of Dbp9p

DBP9 was amplified by PCR using a high fidelity DNA polymerase (*Pfu Turbo*™ DNA polymerase, Stratagene), plasmid YCplac33-*DBP9* as the template, and the primer couple DBP9-G1 and DBP9-G2 to introduce an in-frame *Sal*I restriction site. The PCR product was digested with *Sal*I, *Hin*dIII, and *Acc*I. A 1.07-kb *Sal*I/*Hin*dIII fragment containing the 5′ half of the *DBP9* ORF was gel purified and subcloned into the *Sal*I/*Hin*dIII-restricted plasmid pAS24 (Schmidt et al., 1997), yielding the plasmid pAS24-5′*DBP9*. A 1.1-kb *Hin*dIII insert from YCplac33-*DBP9*, containing the 3′ part of *DBP9*, was then subcloned into the *Hin*dIII-restricted plasmid pAS24-5′-*DBP9*, yielding the plasmid pAS24-*DBP9* (pMCD9-6), in which the expression of *HA-DBP9* is under the control of the *GAL1-10* promoter.

The *GAL::DBP9* strain was obtained after transformation of MCD9H-2D [YCplac33-*DBP9*] with pAS24-*DBP9* and plasmid shuffling on SGal-Leu plates containing 5-FOA. Growth behavior on galactose and glucose media was further studied to test the faithful complementation and the shut-off under nonpermissive conditions.

For in vivo depletion, the *GAL::DBP9* strain was grown in YPGal medium at 30 °C until midexponential phase ($OD_{600} = 1$) and then inoculated in YPD medium. Cell growth was monitored over a period of 36 h during which the culture was regularly diluted into fresh YPD medium to maintain exponential growth. At different time points, samples were taken to perform protein and RNA extractions, and polysome analysis.

Generation of plasmid-borne *dbp9* mutant alleles by PCR-random mutagenesis

Slow-growth (sg) and temperature-sensitive (ts) *dbp9* alleles were generated by random PCR mutagenesis. Briefly, 16 independent PCRs using Taq DNA polymerase (Gibco, BRL), M13/pUC sequencing and reverse sequencing primers (New England BioLabs), and as template the plasmid YCplac111-*HA-DBP9*, were performed under conditions where one dNTP is present in decreasing amounts (175 μM, 150 μM, 125 μM, and 100 μM, done separately for the four dNTPs). The PCR products were pooled, digested with *Bam*HI and *Eco*RI, gel purified, and cloned as a 2.34-kb fragment into the *Bam*HI/*Eco*RI-restricted plasmid YCplac111-*HA-DBP9*. In a first round of transformation, around 7,000 *E. coli* transformants were obtained from which plasmid DNA was prepared and transformed into MCD9H-2D [YCplac33-*DBP9*]. A total of 5,000 yeast transformants were obtained on SD-Leu plates at 30 °C and were subsequently replica plated at the same time on SD-Leu and 5-FOA-containing plates at 30 °C, 18 °C, and 37 °C. Candidates showing differential growth on 5-FOA-containing plates regarding the temperature of incubation were first confirmed by restreaking at all three temperatures. In a second time, their plasmid DNA was extracted (Ward, 1990), amplified in *E. coli*, and back transformed into MCD9H-2D [YCplac33-*DBP9*]. Upon plasmid shuffling, six *dbp9* alleles were finally retained. The following plasmids bearing *dbp9* alleles were used in this study: YCplac111-*HA-dbp9-1* (pMCD9-7; slight sg at 30 °C, ts at 37 °C), YCplac111-*HA-dbp9-3* (pMCD9-9; tight ts at 37 °C) and YCplac111-*HA-dbp9-5* (pMCD9-11; sg at 30 °C, tight ts at 37 °C).

Isolation of *dbp6-13* multicopy suppressors

The ts strains YDK9-2C (*MATα dbp6*::HIS3MX6 pRS416-*dbp6-13*) and YDK9-2D (*MAT***a** *dbp6*::HIS3MX6 pRS416-*dbp6-13*) were transformed with a YEplac181-based yeast genomic library. The cells were then grown for 3 h in liquid YPD medium at 30 °C and subsequently plated on SD-Leu plates. After a 2-h incubation at the permissive temperature (30 °C), the plates were incubated for 4 days at the nonpermissive temperature (35 °C). To exclude transformants that received library-borne *DBP6*, cells from colonies that grew at 35 °C were streaked on 5-FOA-containing plates. Only those candidates unable to segregate the resident plasmid were selected for further analysis. From a total of approximately

60,000 transformants, the wild-type *DBP6* gene was recovered around 25 times whereas only two weakly suppressing clones were obtained. Library plasmids were isolated (Ward, 1990), and restriction analysis indicated that the two clones were likely to be identical. Sequencing into one of the two clones revealed the presence of the two complete ORFs, *DBP9* and *YSH1*. Transforming the *dbp6-13* mutant with YEplac181-*DBP9* (pMCD9-3), which only contains the *DBP9* ORF, showed that *DBP9* alone was sufficient to confer suppression.

Synthetic interaction crosses

For the construction of the different *dbp6/dbp9* double mutants, YDK8-1A (*MAT*α *dbp6*::kanMX4) pRS416-*DBP6* was crossed to MCD9H-4C (*MAT***a** *dbp9*::HIS3MX6) bearing the plasmids YCplac111-*HA-dbp9-1*, *-3*, or *-5*, and the resulting diploid strains YDK33 (*MAT***a**/α *dbp6*::kanMX4/*DBP6 dbp9*::HIS3MX6/*DBP9* pRS416-*DBP6* YCplac111-*HA-dbp9-1*), YDK34 (*MAT***a**/α *dbp6*::kanMX4/*DBP6 dbp9*::HIS3MX6/*DBP9* pRS416-*DBP6* YCplac111-*HA-dbp9-3*), and YDK36 (*MAT***a**/α *dbp6*::kanMX4/*DBP6 dbp9*::HIS3MX6/*DBP9* pRS416-*DBP6* YCplac111-*HA-dbp9-5*) were sporulated and tetrads were dissected. To obtain different double mutant combinations, the spore clones YDK33-8C (*MAT***a** *dbp6*::kanMX4 *dbp9*::HIS3MX6 pRS416-*DBP6* YCplac111-*HA-dbp9-1*), YDK34-4C (*MAT*α *dbp6*::kanMX4 *dbp9*::HIS3MX6 pRS416-*DBP6* YCplac111-*HA-dbp9-3*), and YDK36-26C (*MAT***a** *dbp6*::kanMX4 *dbp9*::HIS3MX6 pRS416-*DBP6* YCplac111-*HA-dbp9-5*) were transformed with the plasmids pRS414-*dbp6-2*, pRS414-*dbp6-3*, pRS414-*dbp6-4*, and pRS414-*dbp6-13* and subjected to plasmid shuffling on 5-FOA-containing plates. No viable *dbp6-4/dbp9* and *dbp6-13/dbp9* double mutants could be recovered, indicating that both the *dbp6-4* and *dbp6-13* mutations were conferring synthetic lethality to the *dbp9-1*, *-3*, and *-5* mutants. On the other hand, viable, albeit slow-growing, *dbp6-2/dbp9* and *dbp6-3/dbp9* double mutants could be recovered, which showed that the milder *dbp6-2* and *dbp6-3* alleles were strongly synthetically enhancing the moderate growth defect of the *dbp9-1*, *-3*, and *-5* mutants (see Results).

Two-hybrid interaction analysis

The positive and negative control plasmids pVA3-1 (GAL4 DNA-BD, murine p53), pTD1-1 (GAL4 AD, SV40 large T-antigen), and pLAM5′-1 (GAL4 DNA-BD, human lamin C) are from Clontech and the reporter strain PJ69-4A (*MAT***a** *trp1-901 leu2-3,112 ura3-52 his3-200 gal4*Δ *gal80*Δ *LYS2::GAL1-HIS3 GAL2-ADE2 met2::GAL7*-lacZ) has been described (James et al., 1996). The complete *DBP6*, *DBP9*, *SPB4*, and *FAL1* ORFs and their cognate terminators were cloned into the GAL4 AD fusion plasmid pACTII (Clontech) and into the GAL4 DNA-BD fusion plasmid pAS2$\Delta\Delta$ (Fromont-Racine et al., 1997); the PCR-derived sequences were verified by sequencing. All plasmids were shown to complement their respective null mutations to the wild-type extent, and expression of the respective GAL4 AD fusion proteins was confirmed by western blotting using the 16B12 anti-HA antibodies. Details on the construction of the two-hybrid plasmids can be obtained upon request.

Sucrose gradient analyses

Polysome analyses and ribosomal subunit quantifications were performed as previously described (Kressler et al., 1997).

RNA analysis

Pulse-chase labeling of pre-rRNA and RNA preparations was performed as described previously (Kressler et al., 1998). Steady-state levels of pre-rRNAs were assessed by northern and primer extension analyses according to Venema et al. (1998). For the primer extension performed with the primer I, a 10-fold molar excess of cold primer was mixed with the radiolabeled primer immediately before annealing. The oligonucleotides used for northern analysis and primer extension were as previously described (Burger et al., 2000) except for oligonucleotide I which is described in Table 2. For the location of the oligonucleotides see Figure 1.

In situ localization of HA-Dbp9p

A plasmid-borne, HA epitope-tagged *DBP9* allele was constructed by fusion PCR (Ho et al., 1989). Briefly, two DNA fragments (A and B) with sequence overlap were generated in a first PCR series using *Pfu* polymerase, the plasmid YCplac33-*DBP9* as the template, and the two primer couples described in Table 2: DBP9-P3 and DBP9-P4 and DBP9-P5 and a 24-mer reverse sequencing primer (−48; New England Biolabs). The fusion PCR was performed using the gel-purified fragments A and B as templates and the primers DBP9-P4 and the reverse sequencing primer. A 1.54-kb *Pst*I/*Bsp*EI DNA fragment from the fusion PCR product, containing the *DBP9* promoter region, the HA epitope, and the 65 first codons of *DBP9* ORF, was subcloned into the *Pst*I/*Bsp*EI-restricted plasmid YCplac111-*DBP9* (pMCD9-2), yielding the plasmid YCplac111-*HA-DBP9* (pMCD9-4). The *HA-DBP9* strain was obtained after transformation of MCD9H-2D [YCplac33-*DBP9*] with YCplac111-*HA-DBP9* and plasmid shuffling on SD-Leu plates containing 5-FOA. The plasmid-borne *HA-DBP9* allele complemented the *dbp9*-null allele to the wild-type extent under all tested conditions. Western blot analysis with monoclonal mouse anti-HA antibodies detected a single protein, migrating at the expected molecular mass of 70 kDa, in whole cell lysates of the *HA-DBP9* strain, but not of the control *DBP9* strain.

Indirect immunofluorescence analyses were performed with the *HA-DBP9* strain as previously described (Kressler et al., 1998), except that the secondary antibodies were goat anti-mouse fluorescein-conjugated antibodies and goat anti-rabbit rhodamine-conjugated antibodies (dilution 1/200, Pierce).

ACKNOWLEDGMENTS

We acknowledge Monique Doère for excellent technical assistance and Marion Schmidt-Zachmann for providing the NOH61 cDNA. We are grateful to Jesús de la Cruz for careful reading of the manuscript. We are grateful to Costa Georgopoulos for support. This work has been funded by a grant from the Swiss National Science Foundation (to PL).

Received May 10, 2001; manuscript accepted without revision June 5, 2001

REFERENCES

Aitchison JD, Rout MP. 2000. The road to ribosomes. Filling potholes in the export pathway. *J Cell Biol 151*:F23–F26.

Ban N, Nissen P, Hansen J, Moore PB, Steitz TA. 2000. The complete atomic structure of the large ribosomal subunit at 2.4 Å resolution. *Science 289*:905–920.

Bergès T, Petfalski E, Tollervey D, Hurt EC. 1994. Synthetic lethality with fibrillarin identifies NOP77p, a nucleolar protein required for pre-rRNA processing and modification. *EMBO J 13*:3136–3148.

Bird LE, Subramanya HS, Wigley DB. 1998. Helicases: A unifying structural theme? *Curr Opin Struct Biol 8*:14–18.

Burger F, Daugeron M-C, Linder P. 2000. Dbp10p, a putative RNA helicase from *Saccharomyces cerevisiae*, is required for ribosome biogenesis. *Nucleic Acids Res 28*:2315–2323.

Chen JY-F, Stands L, Staley JP, Jackups RR Jr, Latus LJ, Chang T.-H. 2001. Specific alterations of U1-C protein or U1 small nuclear RNA can eliminate the requirement of Prp28p, an essential DEAD box splicing factor. *Mol Cell 7*:227–232.

Colley A, Beggs J, Tollervey D, Lafontaine DLJ. 2000. Dhr1p, a putative DEAH-box RNA helicase is associated with the box C+D snoRNA U3. *Mol Cell Biol 20*:7238–7246.

Daugeron MC, Linder P. 1998. Dbp7p, a putative ATP-dependent RNA helicase of *Saccharomyces cerevisiae* is required for 60S ribosomal subunit assembly. *RNA 4*:566–581.

de la Cruz J, Kressler D, Linder P. 1999. Unwinding RNA in *Saccharomyces cerevisiae*: DEAD-box proteins and related families. *Trends Biochem Sci 24*:192–198.

de la Cruz J, Kressler D, Rojo M, Tollervey D, Linder P. 1998. Spb4p, an essential putative RNA helicase, is required for a late step in the assembly of 60S ribosomal subunits in *Saccharomyces cerevisiae*. *RNA 4*:1268–1281.

Eichler DC, Craig N. 1994. Processing of eukaryotic ribosomal RNA. *Prog Nucleic Acid Res Mol Biol 49*:197–239.

Fromont-Racine M, Rain JC, Legrain P. 1997. Toward a functional analysis of the yeast genome through exhaustive two-hybrid screens. *Nature Genet 16*:277–282.

Fuller-Pace FV, Nicol SM, Reid AD, Lane DP. 1993. DbpA: A DEAD box protein specifically activated by 23S rRNA. *EMBO J 12*:3619–3626.

Gietz D, St Jean A, Woods RA, Schiestl RH. 1992. Improved method for high efficiency transformation of intact yeast cells. *Nucleic Acids Res 20*:1425.

Gietz RD, Sugino A. 1988. New yeast–*Escherichia coli* shuttle vectors constructed with in vitro mutagenized yeast genes lacking six-base pair restriction sites. *Gene 74*:527–534.

Ho JH, Kallstrom G, Johnson AW. 2000. Nmd3p is a Crm1p-dependent adapter protein for nuclear export of the large ribosomal subunit. *J Cell Biol 151*:1057–1066.

Ho SN, Hunt HD, Horton RM, Pullen JK, Pease LR. 1989. Site-directed mutagenesis by overlap extension using the polymerase chain reaction. *Gene 77*:51–59.

Hügle B, Scheer U, Franke WW. 1985. Ribocharin: A nuclear Mr 40,000 protein specific to precursor particles of the large ribosomal subunit. *Cell 41*:615–627.

Iost I, Dreyfus M, Linder P. 1999. Ded1p, a DEAD-box protein required for translation initiation in *Saccharomyces cerevisiae*, is an RNA helicase. *J Biol Chem 274*:17677–17683.

James P, Halladay J, Craig EA. 1996. Genomic libraries and a host strain designed for highly efficient two-hybrid selection in yeast. *Genetics 144*:1425–1436.

Jamieson DJ, Beggs JD. 1991. A suppressor of yeast *spp81/ded1* mutations encodes a very similar putative ATP-dependent RNA helicase. *Mol Microbiol 5*:805–812.

Jankowsky E, Gross CH, Shumann S, Pyle AM. 1999. The DexH protein NPH-II is a processive and directional molecular motor for unwinding RNA. *Nature 403*:447–451.

Jankowsky E, Gross CH, Shumann S, Pyle AM. 2001. Active disruption of an RNA–protein interaction by a DExH/D RNA helicase. *Science 291*:121–125.

Kaiser C, Michaelis S, Mitchell A. 1994. In: *Methods in yeast genetics: A Cold Spring Harbor Laboratory course manual.* Cold Spring Harbor, New York: Cold Spring Harbor Laboratory Press.

Kistler AL, Guthrie C. 2001. Deletion of MUD2, the yeast homolog of U2AF65, can bypass the requirement for Sub2, an essential spliceosomal ATPase. *Genes & Dev 15*:42–49.

Kressler D, de la Cruz J, Rojo M, Linder P. 1997. Fal1p is an essential DEAD-box protein involved in 40S-ribosomal-subunit biogenesis in *Saccharomyces cerevisiae*. *Mol Cell Biol 17*:7283–7294.

Kressler D, de la Cruz J, Rojo M, Linder P. 1998. Dbp6p is an essential putative ATP-dependent RNA helicase required for 60S-ribosomal-subunit assembly in *Saccharomyces cerevisiae*. *Mol Cell Biol 18*:1855–1865.

Kressler D, Doère M, Rojo M, Linder P. 1999a. Synthetic lethality with conditional *dbp6* alleles identifies Rsa1p, a nucleoplasmic protein involved in the assembly of 60S ribosomal subunits. *Mol Cell Biol 19*:8633–8645.

Kressler D, Linder P, de la Cruz J. 1999b. Protein *trans*-acting factors involved in ribosome biogenesis in *Saccharomyces cerevisiae*. *Mol Cell Biol 19*:7897–7912.

Kressler D, Rojo M, Linder P, de la Cruz J. 1999c. Spb1p is a putative methyltransferase required for 60S ribosomal subunit biogenesis in *Saccharomyces cerevisiae*. *Nucleic Acids Res 27*:4598–4608.

Liang W-Q, Clark JA, Fournier MJ. 1997. The rRNA-processing function of the yeast U14 small nucleolar RNA can be rescued by a conserved RNA helicase-like protein. *Mol Cell Biol 17*:4124–4132.

Linder P, Tanner NK, Banroques J. 2001. From RNA helicases to RNPases. *Trends Biochem Sci 26*:339–341.

Lorsch JR, Herschlag D. 1998a. The DEAD box protein eIF4A. 1. A minimal kinetic and thermodynamic framework reveals coupled binding of RNA and nucleotide. *Biochemistry 37*:2180–2193.

Lorsch JR, Herschlag D. 1998b. The DEAD box protein eIF4A. 2. A cycle of nucleotide and RNA-dependent conformational changes. *Biochemistry 37*:2194–2206.

Lundblad V. 1994. *Saccharomyces cerevisiae*. In: Ausubel FM, Brent R, Kingston RE, Moore DD, Seidman JG, Smith JA, Struhl K (eds.). *Current protocols in molecular biology.* New York: John Wiley & Sons, Inc.

Mélèse T, Xue Z. 1995. The nucleolus: An organelle formed by the act of building a ribosome. *Curr Opin Cell Biol 7*:319–324.

Nissen P, Hansen J, Ban N, Moore PB, Steitz TA. 2000. The structural basis of ribosome activity in peptide bond synthesis. *Science 289*:920–930.

O'Day C-L, Dalbadie-McFarland G, Abelson J. 1996. The *Saccharomyces cerevisiae* Prp5 protein has RNA-dependent ATPase activity with specificity for U2 small nuclear RNA. *J Biol Chem 271*:33261–33267.

Olson MO, Dundr M, Szebeni A. 2000. The nucleolus: An old factory with unexpected capabilities. *Trends Cell Biol 10*:189–196.

Planta RJ, Mager WH. 1998. The list of cytoplasmic ribosomal proteins of *Saccharomyces cerevisiae*. *Yeast 14*:471–477.

Sambrook J, Fritsch EF, Maniatis T. 1989. *Molecular cloning: A laboratory manual.* Cold Spring Harbor, New York: Cold Spring Harbor Laboratory Press.

Scheer U, Hock R. 1999. Structure and function of the nucleolus. *Curr Opin Cell Biol 11*:385–390.

Schmidt A, Bickle M, Beck T, Hall MN. 1997. The yeast phosphatidylinositol kinase homolog TOR2 activates RHO1 and RHO2 via the exchange factor ROM2. *Cell 88*:531–542.

Schwer B. 2001. A new twist on RNA helicases: DExH/D box proteins as RNPases. *Nature Struct Biol 8*:113–116.

Sikorski RS, Hieter P. 1989. A system of shuttle vectors and yeast host strains designed for efficient manipulation of DNA in *Saccharomyces cerevisiae*. *Genetics 122*:19–27.

Staley JP, Guthrie C. 1998. Mechanical devices of the spliceosome: Motors, clocks, springs, and things. *Cell 92*:315–326.

Sun C, Woolford JL Jr. 1994. The yeast *NOP4* gene product is an essential nucleolar protein required for pre-rRNA processing and accumulation of 60S ribosomal subunits. *EMBO J 13*:3127–3135.

Thomas BJ, Rothstein R. 1989. Elevated recombination rates in transcriptionally active DNA. *Cell 56*:619–630.

Trapman J, Planta RJ. 1976. Maturation of ribosomes in yeast. I. Kinetic analysis by labelling of high molecular weight rRNA species. *Biochim Biophys Acta 442*:265–274.

Trapman J, Planta RJ, Raué HA. 1976. Maturation of ribosomes in yeast. II. Position of the low molecular weight rRNA species in the maturation process. *Biochim Biophys Acta 442*:275–284.

Trapman J, Retèl J, Planta RJ. 1975. Ribosomal precursor particles from yeast. *Exp Cell Res 90*:95–104.

Udem SA, Warner JR. 1973. The cytoplasmic maturation of a ribo-

somal precursor ribonucleic acid in yeast. *J Biol Chem 248*:1412–1416.
Venema J, Bousquet-Antonelli C, Gelugne J-P, Caizergues-Ferrer M, Tollervey D. 1997. Rok1p is a putative RNA helicase required for rRNA processing. *Mol Cell Biol 17*:3398–3407.
Venema J, Planta RJ, Raué HA. 1998. In vivo mutational analysis of ribosomal RNA in *Saccharomyces cerevisiae.* In: Martin R, ed. *Protein synthesis: Methods and protocols.* Totowa, NJ: Humana Press. pp 257–270.
Venema J, Tollervey D. 1999. Ribosome biosynthesis in *Saccharomyces cerevisiae*. *Annu Rev Genet 33*:261–331.
Wach A, Brachat A, Pöhlmann R, Philippsen P. 1994. New heterologous modules for classical or PCR-based gene disruptions in *Saccharomyces cerevisiae*. *Yeast 10*:1793–1808.
Ward A. 1990. Single-step purification of shuttle vectors from yeast for high frequency back-transformation into *E. coli*. *Nucleic Acids Res 18*:5319.
Warner JR. 1999. The economics of ribosome biosynthesis in yeast. *Trends Biochem Sci 24*:437–440.
Woolford JL Jr, Warner JR. 1991. The ribosome and its synthesis. In: Broach JR, Pringle JR, Jones EW eds. *The molecular and cellular biology of the yeast Saccharomyces: Genome dynamics, protein synthesis, and energetics.* Cold Spring Harbor, New York: Cold Spring Harbor Laboratory Press. pp 587–626.
Zanchin NIT, Goldfarb DS. 1999. Nip7p interacts with Nop8p, an essential nucleolar protein required for 60S ribosome biogenesis, and the exosome subunit Rrp43p. *Mol Cell Biol 19*:1518–1525.
Zirwes RF, Eilbracht J, Kneissel S, Schmidt-Zachmann MS. 2000. A novel helicase-type protein in the nucleolus: Protein NOH61. *Mol Biol Cell 11*:1153–1167.